Identifying the Requirement and Mechanism of the Dynamic Yet Kinetically Stable ClpXP Interface

By

Alvaro Jorge Amor

B.S., Biochemistry and Molecular Biology (BCMB)
Ursinus College – 2012

SUBMITTED TO THE DEPARTMENT OF BIOLOGY IN PARTIAL FULFILLMENT OF
THE REQUIREMENTS FOR THE DEGREE OF

DOCTOR OF PHILOSOPHY
AT THE
MASSACHUSETTS INSTITUTE OF TECHNOLOGY

July 2017   [September 2017]

Signature of Author_____

Signature redacted

Department of Biology
June 6, 2017

Certified by_____

Signature redacted

Robert T. Sauer
Salvador E. Luria Professor of Biology
Thesis Supervisor

Accepted by_____

Signature redacted

Amy E. Keating
Professor of Biology
Co-Chairman, Biology Graduate Committee

Identifying the Requirement and Mechanism of the Dynamic Yet Kinetically Stable ClpXP Interface

By

Alvaro Jorge Amor

Submitted to the Department of Biology on 7/14/2017
in partial fulfillment of the requirements for the degree of Doctor of Philosophy at the
Massachusetts Institute of Technology

ABSTRACT

AAA+ (ATPases Associated with various cellular Activities) proteases carry out regulated degradation and protein quality control. To achieve these goals, a barrel-shaped peptidase, with active sites in a sequestered chamber, cooperates with an attached AAA+ hexamer that recognizes, unfolds and translocates the protein substrate into the degradation chamber. The interaction between the AAA+ hexamer and peptidase must be specific and stable enough to ensure efficient degradation. However, information about the assembly of these proteases is limited. The subject of this thesis is the AAA+ ClpXP protease from *Escherichia coli*. ClpX is a AAA+ hexamer, and ClpP is a self-compartmentalized peptidase. Previous experiments have shown that ATP is required for assembly of active ClpXP complexes. Moreover, the IGF loops of ClpX are known to be important for stabilizing assembly.

In Chapter 2, I use bio-layer interferometry (BLI) to determine the rates of ClpXP assembly and disassembly under different nucleotide conditions. ATP or ATPγS, a slowly hydrolyzed derivative, must occupy at least a subset of ClpX subunits allow ClpP binding. Moreover, I find that ClpX can only dissociate from ClpP once bound ATP is hydrolyzed to ADP and inorganic phosphate. As long as ClpX is ATP-bound, the ClpXP complex remains kinetically stable for more than three hours. However, even in the presence of ATP, the complex dissociates rapidly when ADEP, a small-molecule mimic of the IGF loop, is added. These results imply that the ClpXP interface is highly dynamic, with individual IGF-loops constantly unbinding and rebinding ClpP.

In Chapter 3, I probe why ATP is important for ClpP binding and interrogate the importance of the sequence, length, and number of IGF-loops in ClpP binding. I found that ATP/ATPγS does not change the exposure of the IGF-loops but rather their proximity. At least four loops are required for stable binding, the length of the IGF loop is important, and residues in addition to the actual IGF sequence also play a role in complex stability. Finally, I discovered that a full complement of IGF loops is important both to allow rapid degradation and for degradation processivity because mutants with less than six loops do not appear to fully open the ClpP pore.

Thesis Advisor: Robert T. Sauer

ACKNOWLEDGEMENTS

It would be a lie to say that my Ph.D. was a solo effort. It took the tremendous support of advisors, colleagues, friends, and family to make these five years end so well.

First, I would like to give many, many thanks to my advisor Bob Sauer. His advice, scientific and otherwise, has been invaluable in providing guidance. None of my scientific success would have been possible without him, and it was his continuation to challenge me that made me a much, much better scientist than when I started. I can only hope to take what I learned from him and only become better. My true gratitude could not be put into words.

Tania Baker, my co-advisor, was also invaluable. Through joint meetings and discussion, she brought fresh perspective and ideas that led to successful experiments, faster troubleshooting, and was a pleasure to write papers with. Between her and Bob, I couldn't have had a better co-advised doctorate experience.

My committee, Amy Keating and Thomas Schwartz, were also incredibly instrumental, not simply for tracking my progress but for providing a fresh scientific perspective when I presented setbacks at our annual meetings. Additionally, they were very good at giving me a headache during my qualifying exam.

Most of my successful scientific work was carried out in the Biophysical Instrumentation Facility (BIF), which houses the Octet-Red 96 platform. This is made available through the efforts of Barbara Imperiali, who I'd like to thank for making such a great facility available. I'd also like to thank Debby Pheasant, who manages it and has been great to talk to over the years and long hours spent at the BIF.

My colleagues on the 5th floor are simply the best. In the Sauer lab, the passage of many grad students and post docs has been nothing but a pleasure to work with, and have been friends throughout the years. I'd like to specifically thank Ben Stinson, who got my ClpXP work started from my early days of failed experiments. I also like to thank Karl Schmitz, who has been a fantastic collaborator and friend over the course of my doctorate.

I'd like to thank my family. My parents and sister have done nothing but support me when at times I've fallen off the face of the earth. I don't deserve their love, but I'm glad I have it. As much as the people at MIT have made this PhD possible, I give my family equal credit.

Finally, I'd like to thank my friends of past and present, including old friends from my time at Ursinus College to current friends both at MIT and my time in New England. They've done well in supporting me through some rather rough times academically and personally, and are just genuinely fun to have in my life. Probably too much fun... I rather not risk listing them and missing anyone, because too many special people exist in my life and they would know I'd screw it up anyways. You know who you are, and only three of you are reading this anyways. I'll save you three the time and tell you to stop reading here, you probably could be watching Netflix or eating pizza right now, or maybe even doing experiments?

THANKS EVERYONE, ITS BEEN RAD

TABLE OF CONTENTS

LIST OF FIGURES

Chapter One:

Introduction to AAA+ Proteases

Mechanical Work in the Cell. Cells are dynamic entities whose global state frequently changes as a consequence of normal homeostatic needs, development, and responding to environmental stress[1,2]. One method of providing dynamic regulation is physical modification of biomolecules[2,3]. For example, proteins and nucleic acids can be mechanically remodeled, unfolded, and degraded in reactions that utilize ATP hydrolysis to overcome energetic barriers. A classic example of a mechanoenzyme is myosin, which drives muscle contractions. Skeletal myosins II assemble into fibers in which the myosin heads process long stretches of actin through ATP hydrolysis cycles[4]. These actin tracts are attached to other protein complexes that cause this myosin/actin movement to drive myofibril contraction, which in turn leads to muscle fiber contraction[5]. Flagella movement is another example of work, where a series of motor proteins drive movement of a large protein assembly to propel the cell towards or away from specific chemical signals[6]. Finally, the F_1F_o ATP synthase uses mechanical force driven by proton gradients to trigger conformational changes that power ATP synthesis[7].

In this introduction I will describe AAA+ proteases, another type of mechanoenzyme. AAA+ proteases work to carry out regulated proteolysis in the cytosol or organelles of all cells. They recognize and degrade a wide host of substrates, both as a means to regulate levels of certain proteins and as a form of protein quality control. To accomplish these tasks, a AAA+ ring hexamer works to recognize, unfold, and translocate a protein substrate into an associated barrel peptidase, resulting in processive degradation (Figure 1.1). This collaboration requires that the peptidase and AAA+ enzyme maintain contact over hundreds of cycles of ATP hydrolysis, each involving a multitude of conformational changes in the AAA+ machine[8,9].
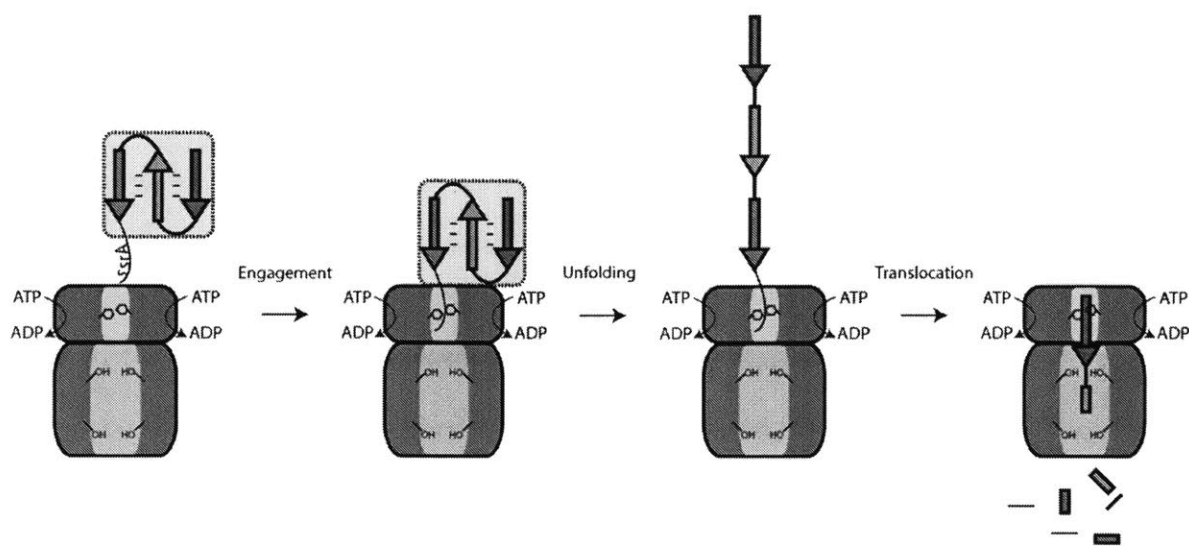
Figure 1.1 Cartoon depicting how the AAA+ protease ClpXP degrades a substrate. In an ATP-dependent step, the axial pore of ClpX (blue) binds an unstructured ssrA degron attached to a protein substrate (grey with multicolored beta-strands). The folded protein is then pulled against the narrow pore, and multiple power strokes, fueled by ATP hydrolysis, result in global protein unfolding[8–11]. Further ATP-hydrolysis cycles drive translocation of the polypeptide chain through the pore and into the proteolysis chamber of the associated ClpP peptidase (orange), where peptidase sites cleave the unfolded protein into peptides.

AAA+ Proteolytic Machines. Proteolytic AAA+ enzymes belong to the **A**TPases **A**ssociated with various cellular **A**ctivities superfamily[12,13], which typically carry out ATP-fueled remodeling of protein and nucleic-acid substrates. ATP-dependent proteases can be further classified into subfamilies, such as ClpXP, ClpAP, HslUV, Lon, FtsH, PAN•20S, the 26S proteasome, etc. The AAA+ portions of these proteolytic machines function as homomeric or heteromeric ring hexamers with an axial pore that plays roles in substrate binding, engagement, and performing mechanical work[14–16]. Each AAA+ subunit minimally consists of two domains: a large domain that contains a Rossman fold (a common ATP binding/hydrolysis motif), and a small helix-rich domain[13,17]. The rigid-body packing of the large subunit of one subunit against the small domain of a neighboring subunit stabilizes the hexameric ring. Within a subunit, ATP

is bound in a crevasse between the large and small AAA+ domains, which are connected by a short hinge region. The orientations of the hinge and both domains change upon ATP hydrolysis and product release, generating conformational changes in the ring that can be coupled to mechanical work[14,18,19]. This labor is typically carried out by pore-1 loops that line the axial pore and contain conserved aromatic residues that are thought to act as molecular paddles that grip polypeptide substrates. ATP-fueled movement of these paddles can move a polypeptide through the pore, allowing processive translocation or transient "tugging" on a native substrate to drive remodeling[20–22].

Like all AAA+ enzymes, proteolytic ring hexamers use conserved sequence motifs, including Walker-A and Walker-B motifs, for binding and hydrolyzing ATP[13,23–25]. The polypeptide backbone of the Walker-A motif or P-loop (GxxxxGK[T/S]) makes hydrogen bonds with the phosphates of ATP/ADP, and the conserved lysine forms a salt bridge with the β phosphate. The Walker-B motif ($\Phi\Phi\Phi\Phi$DE; where Φ is a hydrophobic residue) uses its glutamic acid to activate a water molecule, which then carries out a nucleophilic attack on the γ-phosphate. The sensor-1 motif, commonly containing a polar residue, works with the Walker-B motif to hydrogen bond to water to ready it for nucleophilic attack[26,27]. The sensor-2 motif contributes an arginine to stabilize nucleotide binding by shielding negative charges from the phosphates of the bound ATP[28]. Finally, a conserved residue known as the arginine finger contributes to ATP hydrolysis. Its primary function is to promote hydrolysis in an adjacent subunit by physically entering the ATP-hydrolysis pocket and interacting with bound nucleotide[29,30].

Proteolytic AAA+ enzymes can contain one AAA+ ring (ClpX, HslU, Lon, FtsH, PAN, and the Rpt_{1-6} ring of the 26S proteasome) or two AAA+ rings (ClpA, ClpC, and Cdc48). In the latter

double-ring enzymes, each subunit contains tandem AAA+ modules, which form coaxial N-terminal D1 and C-terminal D2 rings. Compared to single-ring enzymes, double-ring hexamers are generally more stable. The longer axial pore of the double-ring enzymes also provides an opportunity to grip polypeptide substrates more tightly, which may allow unfolding of protein substrates with greater native stability[11,31].

In addition to their conserved large and small domains, proteolytic AAA+ enzymes also contain domains that are only found in specific protease families (Figure 1.2). These extra domains can play roles in regulating ATP hydrolysis, controlling proteolytic activity, tethering specific substrates, or binding adaptor proteins, which in turn can regulate activity or bind specific substrates. Some family-specific domains make contacts that help stabilize the hexameric ring, whereas others simply decorate the periphery of the ring[32–34].
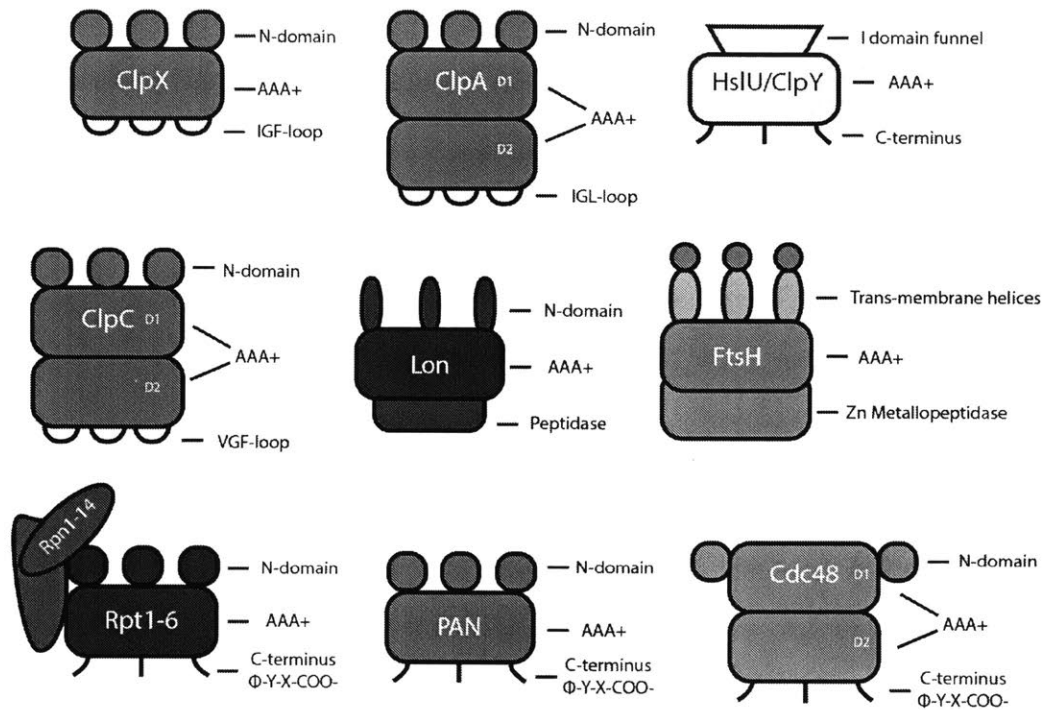
Figure 1.2. Cartoon overview of AAA+ enzymes involved in cellular proteolysis. All of these enzymes contain one or two hexameric rings that bind and hydrolyze ATP in addition to family-specific peripheral domains. ClpX (top left, blue) has peripheral Zn^{2+}-bound N-terminal domains important for substrate/adaptor recognition and IGF-loops that bind ClpP[35,36]. ClpA (top middle, red) is a double-ring enzyme that binds ClpP using IGL loops and has N-domains that bind substrates and adaptors[33,36]. HslU/ClpY (top right, yellow) has substrate gating I-domains, which form a funnel above the axial pore, and C-terminal residues that mediate docking with the HslV/ClpQ peptidase[37,38]. ClpC (middle left, magenta) is another double-ring AAA+ enzyme, similar to ClpA[39]. Lon (middle, purple) contains N-domains that gate substrate as well as assemble Lon into a dimer-of-hexamers[40]. Each Lon subunit also contains a covalently attached peptidase domain (light purple) that forms the peptidase chamber. FtsH (middle right, light blue) is membrane bound through N-terminal transmembrane helices (green and grey). It also encodes a C-terminal metalloprotease domain (orange) that carries out peptide cleavage[41]. The 19S regulatory particle of the 26S proteasome (bottom left, brown and green) contains an Rpt_{1-6} AAA+ ring (brown) and additional subunits that bind and remove ubiquitin (green)[42]. The Rpt_{1-6} subunits use C-terminal Φ-Y-X tripeptides to dock with the 20S peptidase, (ref). Other AAA+ enzymes use similar C-terminal tripeptides to collaborate with 20S, include the single-ring PAN (bottom middle, red), which has an N-terminal domain that stabilizes hexamers, and the double-ring Cdc48 (bottom right, tan), whose N-domains regulate ATP hydrolysis and the affinity of 20S binding[43,44].

AAA+ partner peptidases. The AAA+ components of ATP-dependent proteases function in substrate recognition, unfolding, and translocation. However, a self-compartmentalized peptidase is required for degradation[12,22,33]. All partner peptidases share several features, including assembling into hexameric or heptameric rings that enclose a proteolytic chamber. The active-site residues for peptide cleavage are inside this chamber (Figure 1.1) and therefore can only cleave substrates that gain entry via translocation through the axial pore of the AAA+ ring[45–47]. This general mechanism ensures that cytosolic proteins are only degraded if they are recognized, unfolded, and translocated into the peptidase chamber by a specific AAA+ proteolytic ring.

Despite many general similarities, the peptidases of AAA+ proteases can differ substantially in structure and in active-site mechanism (Figure 1.3)[31]. There is also substantial variation in the mechanisms by which the peptidases interact with their partner AAA+ rings in the active proteolytic machine. For example, in the hexameric Lon and FtsH proteases, the peptidase and AAA+ modules are encoded in a single polypeptide chain[40,41,48]. Thus, upon assembly into the active hexamer, covalent linkage ensures that the AAA+ ring and peptidase ring are properly connected. In other AAA+ proteases, however, the peptidase and AAA+ modules are encoded by different polypeptide chains, requiring non-covalent docking of the AAA+ ring and a peptidase barrel to assemble the active protease. In some of these systems (ClpXP, ClpAP, PAN•20S, and the 26S proteasome), the peptidase barrel is composed of multiple heptameric rings and is two-fold symmetric, and each end of the barrel can dock with a hexameric AAA+ ring, producing a symmetry mismatch[49]. In the HslUV protease, by contrast, the peptidase barrel contains two hexameric rings, which dock symmetrically with one or two hexameric AAA+ rings[38,50]. Whether docking is symmetric or asymmetric, the active proteolytic complexes are stabilized by peripheral interactions from flexible internal loops or C-terminal peptides from the AAA+ ring to

clefts or grooves on the peptidase ring. In addition, axial interactions between the peptidase ring

and AAA+ ring are frequently important for complex stability and function (Figure 1.4)[38,44,51].
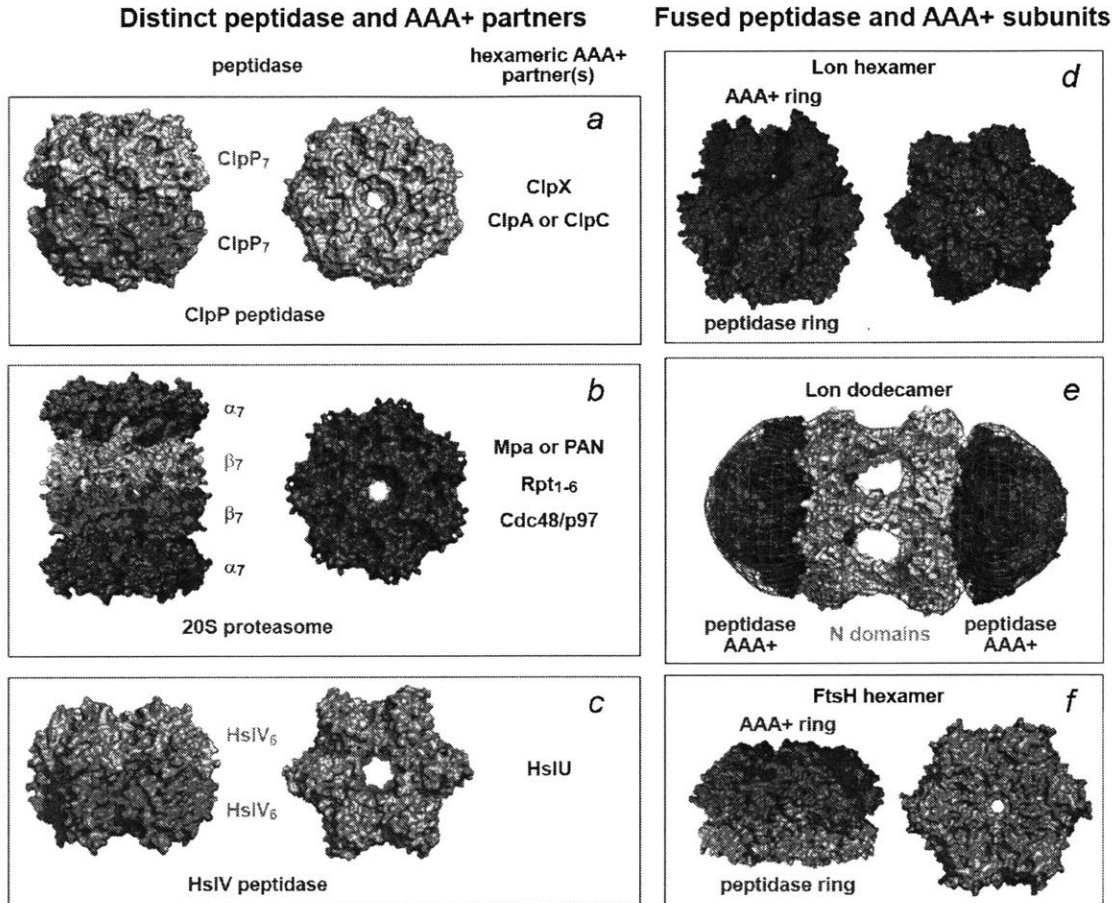
Figure 1.3. Structural overview of the self-compartmental peptidases in AAA+ proteases (adapted from Olivares et al., 2015)[31]. **A.** ClpP (top left, *E. coli*) is a dimer of heptamers that sit tail-to-tail, with serine catalytic triads on the interior of the barrel. **B.** The 20S peptidase (middle left, *Thermoplasma acidophilum*) is comprised of two β-peptidase rings sandwiched between two α gating rings, with each ring being a heptamer. The α and β subunits are identical in bacterial and archaeal assemblies but are each unique in eukaryotes **C.** HslV/ClpQ (bottom left, *Haemophilus influenzae*) is a dodecamer barrel that utilizes an N-terminal threonine as the active-site residue for peptide-bond cleavage[38]. **D.** Lon (top right; *Thermococcus onnurineus*) has the peptidase on the same polypeptide chains as the AAA+ module and uses a Lys-Ser dyad to carry out proteolysis. **E.** Two Lon rings can dimerize via their N domains (middle right, EM

reconstruction[40]) to form a dodecamer with altered enzymatic activity. Notably, the pores formed by N-terminal interactions gate degradation of larger substrates. **F.** FtsH is a homohexameric membrane-bound AAA+ peptidase (bottom right, *Thermotoga maritima*) in which the AAA+ modules and peptidase domains, which utilizes an E-Zn^{2+} mechanism for degrading proteins, are fused.

In all proteases in which the peptidase and AAA+ rings must dock non-covalently, there are three major challenges. First, the interaction must be tight and specific to ensure that the complex does not dissociate partway through degradation of a polypeptide chain. As I show in Chapter 3, premature dissociation results in incomplete and non-processive degradation. Second, the axial pore of the AAA+ ring must line up with the entry pore of the peptidase barrel to ensure a continuous channel for substrate to be spooled into the proteolytic chamber[13,51,52]. Third, the interface between the peptidase barrel must be dynamic and flexible because the AAA+ ring cycles through multiple conformations to carry out ATP-fueled substrate processing. The use of flexible structural elements in the AAA+ ring to dock with the peptidase presumably allows dynamic and multivalent tethering.
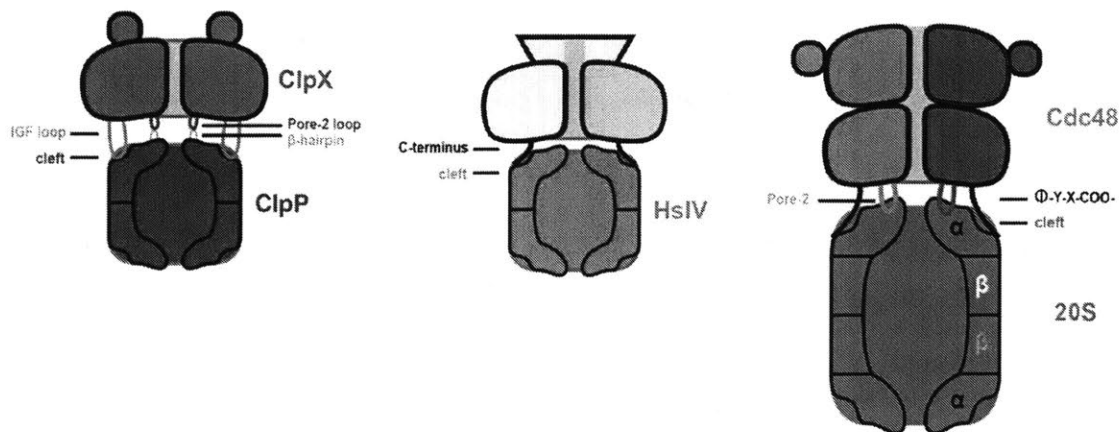
Figure 1.4. Cartoon of noncovalent assemblies for different AAA+ proteases. Left: ClpXP forms contacts through two major binding interactions. Primarily, IGF-bearing loops from ClpX dock into corresponding hydrophobic clefts on ClpP[53]. Although there is a symmetry mismatch between ClpX and ClpP, flexibility of the loop presumably allows for alternative docking events

to take place for the IGF-loop. In addition, the pore-2 loops of ClpX contact N-terminal loops of ClpP[51]. Middle: In HslUV, the C-terminal tails of HslU dock into grooves formed between subunits of HslV. Right: The C-terminal Φ-Y-X tails of Cdc48 dock into to clefts on the α ring of the 20S peptidase, and the pore-2 loops of Cdc48 make additional axial contacts with N-terminal residues from the α-ring[32].

In the sections below, I discuss the major classes of AAA+ proteases that function in bacteria, archaea, and eukaryotes.

Lon and FtsH. As discussed above, the AAA+ modules and peptidase modules are fused in a single polypeptide chain in both the Lon protease and the FtsH protease. Lon is a soluble cytosolic protease, whereas FtsH is a membrane-bound protease[18,54]. Both of these proteases are ubiquitous in the bacterial kingdom, orthologs of Lon are found in archaea and in different organelles of eukaryotes, and orthologs of FtsH are found in mitochondria[55–58].

Cytosolic proteins can become damaged, unfolded, or aggregated as a consequence of cellular stresses, including heat shock, low pH, chemical toxins, and other environmental factors[59–61]. Why protein aggregates are toxic is not completely understood, but all cells have developed mechanisms to try to prevent aggregation or to resolubilize aggregates. Following heat shock of *E. coli*, ~50% of misfolded proteins seem to be degraded by the Lon protease[48,54]. The degrons that target substrates for Lon degradation tend to be hydrophobic and enriched in aromatic residues that would typically be buried in the cores of native proteins[62]. Hence, unfolding of most proteins would expose sequences that allow Lon to recognize and degrade the unfolded protein. For example, a 20-residue sequence that is normally buried in native β-galactosidase becomes exposed upon unfolding and targets the denatured protein for Lon degradation[54,62].

Each subunit of the Lon hexamer contains an N-terminal domain, which appears to play roles in stabilizing the hexamer and recognizing substrate, an AAA+ module, and a C-terminal protease domain that uses a Ser-Lys dyad mechanism for peptide-bond cleavage[40,63]. Interestingly, two Lon hexamers can interact via their N-domains to form a dodecamer[40]. Hexameric and dodecameric Lon are both active proteases, but the hexamer has higher ATPase activity and appears to have a broader repertoire of substrates. In contrast, the dodecamer can degrade small substrates at rates similar to the hexamer but is less active in degrading larger substrates[40]. A low-resolution EM structure of the Lon dodecamer shows that the N-domain interactions form portals with a diameter of ~45 Å (Figure 1.3, panel E) that may restrict access of large substrates to the axial pores of the AAA+ rings[40]. Thus, increases in the intracellular concentration of Lon could stabilize dodecamers, altering its degradation profile.

In *E. coli*, 20-30% of cellular proteins are integrated into the inner and outer cell membranes[64,65]. Inner-membrane proteins are recruited via the SRP/Sec system during synthesis by the ribosome to ensure proper membrane integration[65]. However, ribosome stalling on damaged mRNAs results in addition of the ssrA degron (AANDENYALAA) by the transfer-messenger RNA (tmRNA) system[66]. Many ssrA-tagged cytosolic proteins are degraded by ClpXP, as discussed below, but ssrA-tagged membrane proteins are degraded by FtsH[41]. Additionally, FtsH degrades other membrane proteins, including some whose normal assembly fails. For example SecY is degraded by FtsH when it is not assembled into the SecYEG translocon[67]. Interestingly, FtsH also degrades some soluble cytosolic proteins, such as the heat-shock transcription factor σ^{32}, and thus plays a role in the bacterial response to heat stress[68]. The AAA+ and peptidase domains of the FtsH hexamer are in the cytosol but the AAA+ ring and axial pore are closely opposed to the inner membrane (Figure 1.5). The N-terminal portion of FtsH contains an N-terminal

transmembrane helix, a periplasmic domain that also forms hexamers, and another transmembrane helix that connects to the beginning of the AAA+ domain. The C-terminal peptidase domain, which has a zinc binding motif similar to other metalloproteases, encloses the hexameric proteolytic chamber in combination with the AAA+ domain[69].
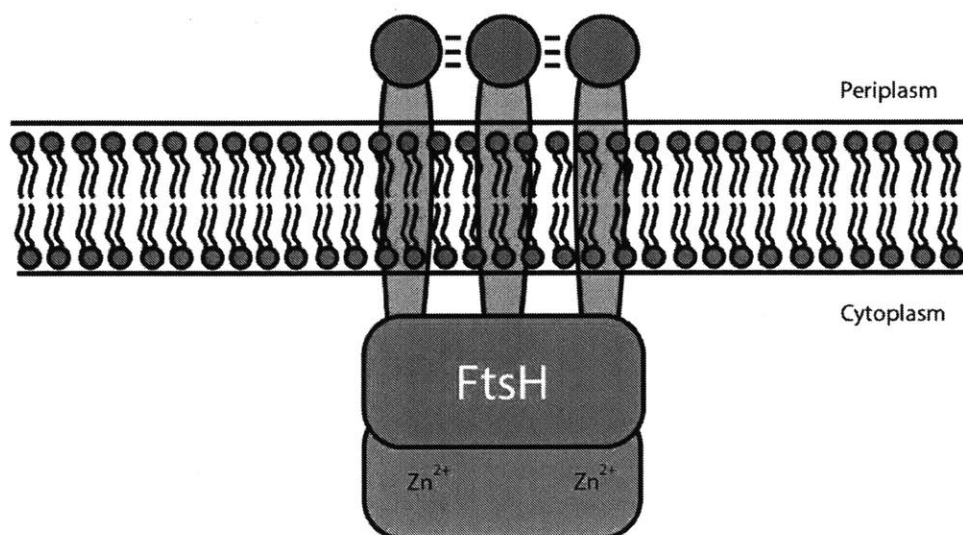
Figure 1.5. Cartoon of membrane-bound FtsH. Transmembrane helices from FtsH anchor into the membrane, and the AAA+ ring and peptidase chamber sit in the cytoplasm. FtsH degrades ssrA-tagged membrane proteins as well as cytoplasmic substrates[41,69].

AAA+ proteases that contain the 20S peptidase. 20S peptidase barrels are found in some bacteria and in archaea and eukaryotes[70]. The 20S particle has a four-ring $\alpha_7\beta_7\beta_7\alpha_7$ structure. The heptameric β-rings contain the peptidase active sites, which utilize an N-terminal threonine as the nucleophile for peptide-bond cleavage[71]. The heptameric α-rings form a narrow portal or gate that prevents entry of peptides larger than ~7 residues into the proteolytic chamber. In some eukaryotes, the gate into the 20S chamber can be opened by the binding of ATP-independent heptamers such as PA28 and PA26, but this mechanism only allows processing of unfolded

polypeptides as native proteins are still too large to enter the chamber[72,73]. 20S degradation of native proteins requires collaboration with AAA+ ring hexamer. In archaea, both a single-ring AAA+ enzyme (PAN) and a double-ring AAA+ enzyme (Cdc48) can dock with 20S and power ATP-dependent protein degradation[32,43]. In actinobacteria, which may have acquired 20S through horizontal gene transfer[74], a PAN homolog, called Mpa or Arc, is responsible for substrate recognition, unfolding, and translocation[75]. In eukaryotes, the 20S peptidase docks with 19S regulatory particles to form the 26S proteasome[76]. Within each 19S particle, six PAN homologs assemble into the AAA+ Rpt_{1-6} ring, which functions analogously to other proteolytic AAA+ enzymes. The 26S proteasome recognizes substrates that have been modified by attachment of multi-chain ubiquitins via the action of E1, E2, and E3 enzymes[77]. The 19S particle contains receptors for binding ubiquitin and for removing the ubiquitins during degradation[78]. In addition to modification by poly-ubiquitins, substrates must contain an unstructured region of polypeptide that can be bound in the axial pore of the Rpt_{1-6} ring[79]. 20S-mediated degradation in archaea and actinobacteria sometimes depends on ubiquitin-like systems in which a small targeting protein is attached to the substrate[75].

The α_7 rings of the 20S peptidase contain clefts that serve as binding sites for tripeptides with the sequence [Φ]-Y-[X] at the extreme C-termini of different partner AAA+ enzymes (the homologous single-ring PAN, Mpa/Arc, and Rpt_{1-6} hexamers and non-homologous double-ring Cdc48 hexamer). These tripeptide motifs are flexibly linked to the small AAA+ domain, presumably allowing six C-terminal tails from the periphery of a hexamer to dock into six of the seven clefts on a heptameric α_7 ring[32,44]. Additional axial interactions between the AAA+

enzyme and the N-terminal twelve residues of each α subunit are also important for formation of the stable protease and gating into the proteolytic chamber[32].

HslUV. The crystal structure of a fully assembled HslUV protease complex has been solved[38]. HslUV contains one or two copies of the AAA+ HslU ring hexamer and the HslV peptidase, a dodecamer consisting of two stacked hexameric rings. HslV subunits are homologous to the β subunits of the 20S peptidase and also use an N-terminal threonine as the active-site nucleophile[38]. Docking between HslU and HslV is mediated by C-terminal peptides from HslU that dock into grooves on the side of an HslV ring[38]. This docking allosterically activates HslV, stabilizing the catalytic sites in their functional conformation. Interestingly, in enzymes containing one HslU hexamer and the HslV dodecamer, only the cis ring of HslV is activated for peptide cleavage[38]. Several specific protein substrates (RscA, SulA, and Arc) have been shown to be degraded by HslUV, but broader rules for substrate recognition have not yet been established[80,81].

During heat shock in *E. coli*, expression of both HslU and HslV increases ~10-fold[50]. Moreover, in biochemical experiments, the rate of HslUV proteolysis increases markedly as temperatures increase from 20 to 55 °C[81]. These facts suggest that HslUV plays a role in the cellular response to heat stress, however redundancy with Lon allows deletion of HslUV to be tolerated under heat shock[82]. The large AAA+ domain of each HslU subunit is interrupted by a family-specific intermediate (I) domain that forms a funnel above the axial pore of the hexamer. Interestingly, mutations in this domain can either abrogate or enhance the rate of ATP hydrolysis, increase or decrease the rates of degradation of specific protein substrates, and change the preferred direction of degradation for substrates with degrons at both the N-terminus and C-terminus[37,83].

These results suggest that the I domain is involved in regulating HslUV activity and substrate recognition.

ClpAP. The ClpAP protease was initially purified based on its biochemical ability to degrade casein, an intrinsically disordered protein, in an ATP-dependent reaction[84]. This AAA+ protease consists of ClpP, a self-compartmentalized peptidase with two heptameric rings stacked back-to-back, and one or two AAA+ ClpA hexamers[85]. I will discuss ClpP later in this chapter. Each ClpA subunit consists of an N-terminal domain and two AAA+ modules, that form D1 and D2 rings in the hexameric enzyme. Early studies showed that ClpAP could degrade different native proteins, including RepA dimers, ssrA-tagged λ repressor, and ssrA-tagged GFP[86–88]. The N-domain of ClpA is flexibly attached to the periphery of the D1 ring but can be deleted without compromising degradation of ssrA-tagged substrates[85,86,89]. Thus, the D1 and D2 rings of ClpA are sufficient for recognition, unfolding, and translocation of ssrA-tagged substrates into ClpP. An important role of the ClpA N-domain is binding to the ClpS adaptor protein[90], which recognizes proteins beginning with N-end rule residues (Phe, Leu, Tyr, and Trp in *E. coli*) and delivers them to ClpAP for degradation[84,33]. Interestingly, ClpS binding to ClpA also suppresses degradation of ssrA-tagged substrates[90].

ClpXP. ClpX, a single-ring AAA+ hexamer, also partners with ClpP to degrade cytoplasmic proteins, including those tagged by the tmRNA system with the ssrA degron[12]. ClpX contains a family-specific N-domain as well as a large and small AAA+ domain. The N-domain, which in isolation is a dimer that binds several structural Zn^{2+} atoms, serves to tether certain substrates and some adaptors to ClpX. For example, the SspB adaptor binds to the N-domain and to part of the ssrA-tag sequence, and thus increases the efficiency with which low concentrations of ssrA-

tagged substrates are degraded by ClpXP[34,91–93]. However, ClpX lacking its N-domain (ClpX$^{\Delta N}$)

is fully active in degradation of higher concentrations of ssrA-tagged proteins and other

substrates that have degrons that can be engaged efficiently by the axial pore of ClpX[46,94].

Numerous structural and biophysical studies have been performed using ClpX$^{\Delta N}$, as deletion of

the N-domain increases enzyme solubility and yield[17,36,85]. More importantly, ClpX$^{\Delta N}$ subunits

can be linked together using genetically encoded tethers to form covalent dimers, trimers and

hexamers [94]. Single-chain ClpX$^{\Delta N}$ pseudohexamers are as active as unlinked ClpX$^{\Delta N}$ hexamers in

supporting degradation by ClpP, and single-chain dimers and trimers, also assemble into fully

active pseudohexamers.

The use of single-chain ClpX$^{\Delta N}$ constructs allows mutations to be engineered into specific

subunits of the hexamer. This topological control allows determination of how many active

subunits and in what configurations are required for ATP hydrolysis and the coupled processes

of mechanical unfolding and translocation of protein substrates[9,14,15,17,51,94]. For example, a

pseudohexamer with only a single hydrolytically active subunit was still able to degrade ssrA-

tagged substrates in an ATP-dependent manner, although slowly. Additionally, a mutant with

only two active subunits had one-third of the activity as a hexamer with six active subunits[94].

These results rule out models in which ClpX must hydrolyze ATP in a concerted fashion or in a

strictly sequential manner and strongly suggest that hydrolysis in the wild-type ring occurs by a

probabilistic or stochastic mechanism. These conclusions are also supported by single-molecule

optical-trapping studies[31,45,95,96]. Nevertheless, there is also evidence for some communication

between subunits in the ring. For example, ATP binding to the ClpX hexamer is positively

cooperative[97].

In certain crystal structures of ClpX pseudohexamers, some subunits adopt a conformation that allows binding of ATP in a cleft between the large and small AAA+ domains (called loadable or L subunits), whereas others adopt conformations that cannot bind ATP (unloadable or U subunits)[9,17]. Most crystal structures have four L subunits and two U subunits arranged in a roughly two-fold symmetric LLULLU arrangement. However, a hexamer in one crystal structure was found to have six L subunits[9,17]. Moreover, solution experiments using a single-chain hexamer with fluorescent dyes in both the large and small AAA+ domains of one subunit, which would quench in the L conformation but not in the U conformation, suggested that the functional hexamer may have five L subunits and one U subunit[9]. Locking one subunit of the hexamer in either the U or in the L conformation using cysteine crosslinking prevented mechanical function but not ATP hydrolysis[9,98]. Why switching between these conformations is functionally important is currently poorly understood.

As noted above, ClpXP degrades many cytoplasmic ssrA-tagged proteins. It also degrades a number of native proteins, including many regulatory proteins and transcription factors, that contain appropriate degrons at either their N-terminal or C-terminal ends[99]. In each case, an unstructured degron binds in the axial pore of the ClpX hexamer, allowing the pore-1 or GYVG loops to grip the substrate[14,45,100]. Attempted translocation of this degron eventually pulls the attached native protein against the pore entry, creating an unfolding force. Depending on the mechanical stability of the native substrate, anywhere from a few power stokes to many hundred power strokes may be required before successful unfolding occurs[8,95,96]. For stable substrates, unfolding is usually the rate-limiting step in overall degradation. However, for relatively unstable substrates, translocation can be rate limiting. In single-molecule optical-trapping studies, both unfolding and translocation can be directly visualized[31,45,96]. Interestingly, even when an average

of 50 or more ATP-hydrolysis events are required, the pre-unfolding dwell times are exponentially distributed, showing that a single power stroke leads to unfolding[96]. This observation suggests that the substrate is only transiently susceptible to unfolding, probably because some thermally inducing fraying of the native structure must occur at the same time as a power stroke. The smallest translocation steps correspond to movement of roughly 5-7 amino acids through the pore, but some steps are two, three, or four times larger, suggesting that power strokes may occur in kinetic bursts that are faster than the response time of the optical trap[96,101].

ClpP and its binding to ClpX or ClpA. As noted above, ClpP is a self-compartmentalized peptidase, which is active as a double-ring tetradecamer. Isolated heptameric rings are inactive, which prevents rouge proteolysis prior to assembly of the 14-mer and enclosure of the degradation chamber[84]. ClpP is the proteolytic component of both ClpXP and ClpAP, and each of its heptameric rings can bind one ClpX or ClpA hexamer. The binding of either ClpX or ClpA to ClpP requires ATP or ATPγS (which is hydrolyzed slowly by ClpX and at an undetectable rate by ClpA), suggesting that ATP hydrolysis is not required for binding. In support of this model, ClpX mutants that cannot hydrolyze ATP are still capable of ATP-dependent stimulation of the peptidase activity of ClpP. This stimulation is observed for peptides larger than 2-3 amino acids and is thought to arise by increasing the size of the ClpP portal and thus allowing larger peptides to diffuse into the proteolytic chamber[52,102,103].

Low-resolution models of ClpXP and ClpAP complexes have been determined by negative-stain electron microscopy, but high-resolution structures are still being pursued. Thus, most of what is known about binding determinants has arisen from bioinformatics, mutational studies, modeling, and biochemistry. To identify potential regions of ClpX and ClpA that might interact with ClpP,

Kim et al. looked for conserved sequences that were absent in HslU, which does not bind ClpP[53].

All ClpX or ClpA orthologs were found to contain a loop region that had an IGF or related

tripeptide motif (e.g., VGF, MGF, IGL, etc.). In ClpX, mutation of either the first or third residue

of this motif prevented functional interactions with ClpP without affecting other ClpX functions,

such as ATP hydrolysis or complex remodeling, as did replacing most of the IGF loop with a

short linker[51,53]. Based on the crystal structure of ClpP and the positions of the IGF loops in a

homology model of ClpX, it was proposed that six IGF tripeptides from a ClpX hexamer could

dock into six hydrophobic clefts on a ClpP ring, leaving one cleft unoccupied. Consistent with

this model, the IGF loop of ClpX could be cleaved by proteases like chymotrypsin, but this

cleavage was blocked by ClpP binding[36]. Both the symmetry mismatch and fact that the IGF

loops are generally disordered in crystal structures suggests that loop flexibility is required for

docking. The postulated interactions between the ClpX IGF loops and ClpP clefts occur on the

peripheries of the hexameric/heptameric rings. Later studies established that there are also axial

interactions between the pore-2 loops of ClpX and the N-terminal hairpins of ClpP, but these

interactions are less energetically important than the peripheral interactions[51].

Interestingly, some bacteria synthesize acyldepsipeptides (ADEPs) that act as mimics of the IGF

loops[52,103]. Crystal structures show that these small molecules bind in the same ClpP clefts as the

IGF loops of ClpX and ClpA[52,103]. ADEP binding to ClpP prevents ClpX or ClpA binding and

causes ordering of the N-terminal residues of ClpP into a β hairpin[52,103] (Figure 1.6). This

conformational change draws the N terminus out of the axial pore, widening it, and turns ClpP

into an unregulated protease of unfolded proteins which *in vivo* causes toxicity[104]. ClpX and

ClpA binding are thought to cause similar portal opening and restructuring of the N-terminal

residues of ClpP, which is probably important to allow efficient translocation of unfolded polypeptides into the degradation chamber.
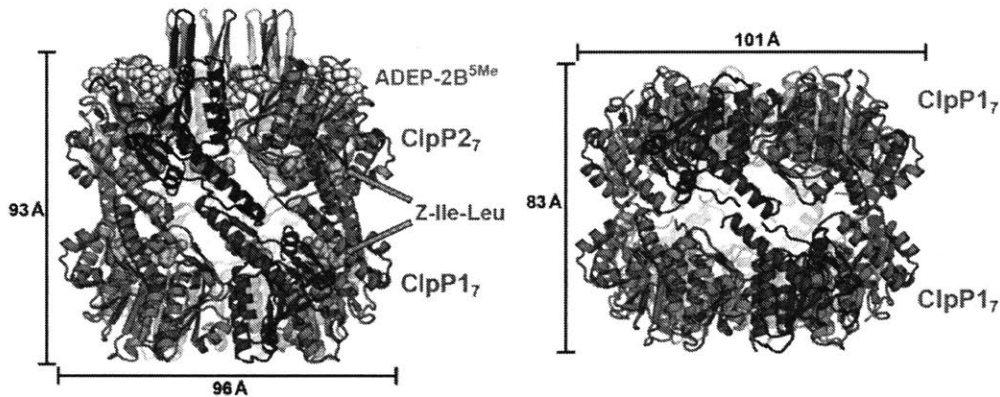
Figure 1.6. Crystal structure of *Mycrobacterium tuberculosis* ClpP with ADEP bound (adapted from Schmitz et al., 2014)[103]. Left: *M. tuberculosis* ClpP is a heterodimer of two genetically distinct ClpP heptamers, ClpP1 and ClpP2. Left. ClpP1P2 crystallized with ADEP-2B[Me] and peptide agonist ZIL. Note that ADEP is only bound to ClpP2, triggering a widening of the axial pore as well as rigidifying the N-terminal residues in a beta-ribbon structure. ClpP1 does not undergo this conformational change. Right: Homomeric ClpP1, crystallized in the presence of ADEP-2B[Me], does not have ADEP bound but displays a compressed structure in which the peptidase catalytic triads assume an inactive conformation.

The peptidase active sites of ClpP contain a conventional Ser-His-Asp catalytic triad, similar to the active site of chymotrypsin. Inactivation of the active site by mutation of the serine to alanine permits proteins unfolded by ClpX or ClpA to be trapped inside the ClpP chamber. This strategy has been used to identify cellular substrates of ClpXP[99,105]. In general, cleavage of a polypeptide chain in the degradation chamber is fast relative to the rates of protein unfolding and translocation, even when some catalytic triads have been inactivated by modification with diisopropylfluorophosphate[105].

Crystal structures show that the ClpP 14-mer can exist in a catalytically active conformation and a compressed conformation in which the active sites are not functional (Figure 1.6, right panel). The relevance of this inactive conformation is unknown. Although it is possible that ClpP changes conformation during ClpXP or ClpAP degradation, electron microscopy studies provide no support for this model.

Over the course of my thesis studies, I have interrogated the nature of the ClpXP interface. By using a method that allows real-time assessment of ClpXP assembly and disassembly kinetics together with mutagenesis and enzymology, I have investigated how the ClpXP interface is established and behaves. In Chapter 2, I discuss how I characterized the interaction of ClpX and ClpP using bio-layer interferometry (BLI). These studies reveal that the complex is very stable as long as ATP is present but becomes unstable in the presence of ADP or the absence of nucleotide. These studies also suggest that the IGF loops are dynamically making and breaking contacts with ClpP. In Chapter 3, I describe experiments in which I probed how different nucleotides affect the accessibility of the IGF loops of ClpX and the distance between these loops. I also characterize the importance of the sequence, length, and number of ClpX IGF loops in binding ClpP and in allowing processive protein degradation.

REFERENCES

1. de Nadal, E., Ammerer, G. & Posas, F. Controlling gene expression in response to stress. *Nat. Rev. Genet.* **12,** 833–45 (2011).

2. Miller, S. B. M., Mogk, A. & Bukau, B. Spatially organized aggregation of misfolded proteins as cellular stress defense strategy. *J. Mol. Biol.* **427,** 1564–1574 (2015).

3. Roberts, A. J., Kon, T., Knight, P. J., Sutoh, K. & Burgess, S. a. Functions and mechanics of dynein motor proteins. *Nat. Rev. Mol. Cell Biol.* **14,** 713–26 (2013).

4.   Geeves, M. A. The dynamics of actin and myosin association and the crossbridge model of muscle contraction. *Biochem. J* **274**, 1–14 (1991).

5.   Mehta, A. D. *et al.* Myosin-V is a processive actin-based motor. *Nature* **400**, 590–3 (1999).

6.   Berg, H. C. The Rotary Motor of Bacterial Flagella. *Annu. Rev. Biochem.* **72**, 19–54 (2003).

7.   Stock, D. Molecular Architecture of the Rotary Motor in ATP Synthase. *Science (80-.).* **286**, 1700–1705 (1999).

8.   Kenniston, J. A., Baker, T. A., Fernandez, J. M. & Sauer, R. T. Linkage between ATP Consumption and Mechanical Unfolding during the Protein Processing Reactions of an AAA+ Degradation Machine. *Cell* **114**, 511–520 (2003).

9.   Stinson, B. M. *et al.* Nucleotide binding and conformational switching in the hexameric ring of a AAA+ machine. *Cell* **153**, 628–639 (2013).

10.   Kenniston, J. A., Baker, T. A. & Sauer, R. T. Partitioning between unfolding and release of native domains during ClpXP degradation determines substrate selectivity and partial processing. *Proc. Natl. Acad. Sci.* **102**, 1390–1395 (2005).

11.   Olivares, A. O., Nager, A. R., Iosefson, O., Sauer, R. T. & Baker, T. a. Mechanochemical basis of protein degradation by a double-ring AAA+ machine. *Nat. Struct. Mol. Biol.* **21**, 871–875 (2014).

12.   Baker, T. a. & Sauer, R. T. ClpXP, an ATP-powered unfolding and protein-degradation machine. *Biochim. Biophys. Acta - Mol. Cell Res.* **1823**, 15–28 (2012).

13.   Hanson, P. I. & Whiteheart, S. W. AAA+ proteins: have engine, will work. *Nat. Rev. Mol. Cell Biol.* **6**, 519–529 (2005).

14.   Iosefson, O., Nager, A. R., Baker, T. a & Sauer, R. T. Coordinated gripping of substrate by subunits of a AAA+ proteolytic machine. *Nat. Chem. Biol.* **11**, 201–206 (2015).

15.   Andreas, M. *et al.* Pore loops of the AAA+ ClpX machine grip substrates to drive translocation and unfolding. *Nat. Struct. Mol. Biol.* **15**, 1147–1151 (2008).

16.   Yamada-Inagawa, T., Okuno, T., Karata, K., Yamanaka, K. & Ogura, T. Conserved Pore Residues in the AAA Protease FtsH Are Important for Proteolysis and its Coupling to ATP Hydrolysis. *J. Biol. Chem.* **278**, 50182–50187 (2003).

17.   Glynn, S. E., Martin, A., Nager, A. R., Baker, T. A. & Sauer, R. T. Structures of Asymmetric ClpX Hexamers Reveal Nucleotide-Dependent Motions in a AAA+ Protein-Unfolding Machine. *Cell* **139**, 744–756 (2009).

18.   Ito, K. & Akiyama, Y. Cellular Functions, Mechanism of Action, and Regulation of Ftsh Protease. *Annu. Rev. Microbiol.* **59**, 211–231 (2005).

19.   Zhao, C., Smith, E. C. & Whiteheart, S. W. Requirements for the catalytic cycle of the N-ethylmaleimide-Sensitive Factor (NSF). *Biochim. Biophys. Acta - Mol. Cell Res.* **1823**, 159–171 (2012).

20. White, S. R. & Lauring, B. AAA+ ATPases: Achieving diversity of function with conserved machinery. *Traffic* **8,** 1657–1667 (2007).

21. LeBowitz, J. H. & McMacken, R. The Escherichia coli dnaB replication protein is a DNA helicase. *J. Biol. Chem.* **261,** 4738–48 (1986).

22. Haslberger, T. *et al.* Protein disaggregation by the AAA+ chaperone ClpB involves partial threading of looped polypeptide segments. *Nat. Struct. Mol. Biol.* **15,** 641–650 (2008).

23. Stratford, F. L. L., Ramjeesingh, M., Cheung, J. C., Huan, L.-J. & Bear, C. E. The Walker B motif of the second nucleotide-binding domain (NBD2) of CFTR plays a key role in ATPase activity by the NBD1-NBD2 heterodimer. *Biochem. J.* **401,** 581–586 (2007).

24. Rai, V., Gaur, M., Shukla, S., Shukla, S., Ambudkar, S.V., Komath, S.S., Prasad, R. Conserved Asp327 of Walker B motif in the N-terminal Nucleotide Binding Domain (NBD-1) of Cdr1p of Candida albicans has acquired a new role in ATP hydrolysis. *Biochemistry* **36,** 490–499 (2010).

25. Walker, J. E., Saraste, M., Runswick, M. J. & Gay, N. J. Distantly related sequences in the alpha- and beta-subunits of ATP synthase, myosin, kinases and other ATP-requiring enzymes and a common nucleotide binding fold. *EMBO J.* **I,** 945–951 (1982).

26. Hattendorf, D. A. *et al.* Cooperative kinetics of both Hsp104 ATPase domains and interdomain communication revealed by AAA sensor-1 mutants. *EMBO J.* **21,** 12–21 (2002).

27. Zeymer, C., Barends, T. R. M., Werbeck, N. D., Schlichting, I. & Reinstein, J. Elements in nucleotide sensing and hydrolysis of the AAA+ disaggregation machine ClpB: A structure-based mechanistic dissection of a molecular motor. *Acta Crystallogr. Sect. D Biol. Crystallogr.* **70,** 582–595 (2014).

28. Hattendorf, D. a & Lindquist, S. L. Analysis of the AAA sensor-2 motif in the C-terminal ATPase domain of Hsp104 with a site-specific fluorescent probe of nucleotide binding. *Proc. Natl. Acad. Sci. U. S. A.* **99,** 2732–2737 (2002).

29. Ogura, T., Whiteheart, S. W. & Wilkinson, A. J. Conserved arginine residues implicated in ATP hydrolysis, nucleotide-sensing, and inter-subunit interactions in AAA and AAA+ ATPases. *J. Struct. Biol.* **146,** 106–112 (2004).

30. Chen, B. *et al.* Engagement of Arginine Finger to ATP Triggers Large Conformational Changes in NtrC1 AAA+ ATPase for Remodeling Bacterial RNA Polymerase. *Structure* **18,** 1420–1430 (2010).

31. Olivares, A. O., Baker, T. A. & Sauer, R. T. Mechanistic insights into bacterial AAA+ proteases and protein-remodelling machines. *Nat. Rev. Microbiol.* **14,** 33–44 (2016).

32. Barthelme, D. & Sauer, R. T. Identification of the Cdc48 • 20. *Science* **337,** 843–847 (2012).

33. Rivera-Rivera, I., Román-Hernández, G., Sauer, R. T. & Baker, T. A. Remodeling of a delivery complex allows ClpS-mediated degradation of N-degron substrates. *Proc. Natl. Acad. Sci. U. S. A.* **111,** E3853-9 (2014).

34.   McGinness, K. E., Bolon, D. N., Kaganovich, M., Baker, T. A. & Sauer, R. T. Altered tethering of the SspB adaptor to the ClpXP protease causes changes in substrate delivery. *J. Biol. Chem.* **282,** 11465–11473 (2007).

35.   Wojtyra, U. a., Thibault, G., Tuite, A. & Houry, W. a. The N-terminal zinc binding domain of ClpX is a dimerization domain that modulates the chaperone function. *J. Biol. Chem.* **278,** 48981–48990 (2003).

36.   Singh, S. K. *et al.* Functional Domains of the ClpA and ClpX Molecular Chaperones Identified by Limited Proteolysis and Deletion Analysis. *J. Biol. Chem.* **276,** 29420–29429 (2001).

37.   Baytshtok, V., Fei, X., Grant, R. A., Baker, T. A. & Sauer, R. T. A Structurally Dynamic Region of the HslU Intermediate Domain Controls Protein Degradation and ATP Hydrolysis. *Structure* **24,** 1766–1777 (2016).

38.   Sousa, M. C. *et al.* Crystal and solution structures of an HslUV protease-chaperone complex. *Cell* **103,** 633–643 (2000).

39.   Liu, J. *et al.* Structural dynamics of the MecA-ClpC complex: A type II AAA+ protein unfolding machine. *J. Biol. Chem.* **288,** 17597–17608 (2013).

40.   Vieux, E. F., Wohlever, M. L., Chen, J. Z., Sauer, R. T. & Baker, T. A. Distinct quaternary structures of the AAA+ Lon protease control substrate degradation. *Proc. Natl. Acad. Sci. U. S. A.* **110,** E2002-8 (2013).

41.   Hari, S. B. & Sauer, R. T. The AAA+ FtsH protease degrades an ssrA-tagged model protein in the inner membrane of Escherichia coli. *Biochemistry* **55,** 5649–5652 (2016).

42.   Huang, X., Luan, B., Wu, J. & Shi, Y. An atomic structure of the human 26S proteasome. *Nat. Struct. Mol. Biol.* **18,** 1–10 (2016).

43.   Smith, D. M. *et al.* ATP binding to PAN or the 26S ATPases causes association with the 20S proteasome, gate opening, and translocation of unfolded proteins. *Mol. Cell* **20,** 687–698 (2005).

44.   Barthelme, D., Chen, J. Z., Grabenstatter, J., Baker, T. A. & Sauer, R. T. Architecture and assembly of the archaeal Cdc48*20S proteasome. *Proc. Natl. Acad. Sci. U. S. A.* **111,** E1687-1694 (2014).

45.   Iosefson, O., Olivares, A. O., Baker, T. A. & Sauer, R. T. Dissection of axial-pore loop function during unfolding and translocation by a AAA+ proteolytic machine. *Cell Rep.* **12,** 1032–1041 (2015).

46.   Martin, A., Baker, T. A. & Sauer, R. T. Diverse Pore Loops of the AAA+ ClpX Machine Mediate Unassisted and Adaptor-Dependent Recognition of ssrA-Tagged Substrates. *Mol. Cell* **29,** 441–450 (2008).

47.   Zhao, C., Slevin, J. T. & Whiteheart, S. W. Cellular functions of NSF: Not just SNAPs and SNAREs. *FEBS Lett.* **581,** 2140–2149 (2007).

48.   Gur, E., Vishkautzan, M. & Sauer, R. T. Protein unfolding and degradation by the AAA+

Lon protease. *Protein Sci.* **21,** 268–278 (2012).

49. Barthelme, D. & Sauer, R. T. Bipartite determinants mediate an evolutionarily conserved interaction between Cdc48 and the 20 *S* peptidase. *Proc. Natl. Acad. Sci.* **110,** 3327–3332 (2013).

50. Rohrwild, M. *et al.* HslV-HslU: A novel ATP-dependent protease complex in Escherichia coli related to the eukaryotic proteasome. *Proc. Natl. Acad. Sci.* **93,** 5808–5813 (1996).

51. Martin, A., Baker, T. a. & Sauer, R. T. Distinct Static and Dynamic Interactions Control ATPase-Peptidase Communication in a AAA+ Protease. *Mol. Cell* **27,** 41–52 (2007).

52. Lee, B.-G. *et al.* Structures of ClpP in complex with acyldepsipeptide antibiotics reveal its activation mechanism. *Nat. Struct. Mol. Biol.* **17,** 471–478 (2010).

53. Kim, Y. I. *et al.* Molecular determinants of complex formation between Clp/Hsp100 ATPases and the ClpP peptidase. *Nat. Struct. Biol.* **8,** 230–233 (2001).

54. Gur, E. & Sauer, R. T. Recognition of misfolded proteins by Lon, a AAA+ protease. *Genes Dev.* **22,** 2267–2277 (2008).

55. Rigas, S., Daras, G., Tsitsekian, D., Alatzas, A. & Hatzopoulos, P. Evolution and significance of the Lon gene family in Arabidopsis organelle biogenesis and energy metabolism. *Front. Plant Sci.* **5,** 1–9 (2014).

56. Fukui, T., Eguchi, T., Atomi, H. & Imanaka, T. A membrane-bound archaeal Lon protease displays ATP-independent proteolytic activity towards unfolded proteins and ATP-dependent activity for folded proteins. *J. Bacteriol.* **184,** 3689–3698 (2002).

57. Bieniossek, C. *et al.* The molecular architecture of the metalloprotease FtsH. *Proc. Natl. Acad. Sci. U. S. A.* **103,** 3066–3071 (2006).

58. Lindahl, M. *et al.* Indentification, characterization, and molecular cloning of a homologue of the bacterial FtsH protease in chloroplast of higher plants. *J. Biol. Chem.* **271,** 229334–293329 (1996).

59. Gidalevitz, T., Prahlad, V. & Morimoto, R. I. The stress of protein misfolding: from single cells to multicellular organisms. *Cold Spring Harb Perspect Biol* **3,** 1–18 (2011).

60. Tyedmers, J., Mogk, A. & Bukau, B. Cellular strategies for controlling protein aggregation. *Nat. Rev. Mol. Cell Biol.* **11,** 777–788 (2010).

61. Li, R., Wu, Z., Wangb, Y., Ding, L. & Wang, Y. Role of pH-induced structural change in protein aggregation in foam fractionation of bovine serum albumin. *Biotechnol. Reports* **9,** 46–52 (2016).

62. Wohlever, M. L., Baker, T. A. & Sauer, R. T. Roles of the N domain of the AAA+ Lon protease in substrate recognition, allosteric regulation and chaperone activity. *Mol. Microbiol.* **91,** 66–78 (2014).

63. Botos, I. *et al.* The Catalytic Domain of Escherichia coli Lon Protease Has a Unique Fold and a Ser-Lys Dyad in the Active Site. *J. Biol. Chem.* **279,** 8140–8148 (2004).

64. Gao, F. P. & Cross, T. a. Recent developments in membrane-protein structural genomics. *Genome Biol.* **6,** 244 (2005).

65. Valent, Q. A. *et al.* The Escherichia coli SRP and SecB targeting pathways converge at the translocon. *EMBO J.* **17,** 2504–2512 (1998).

66. Keiler, K. C., Waller, P. R. & Sauer, R. T. Role of a peptide tagging system in degradation of proteins synthesized from damaged messenger RNA. *Science* **271,** 990–993 (1996).

67. Akiyama, Y., Kihara, A., Tokuda, H. & Ito, K. FtsH (HflB) is an ATP-dependent protease selectively acting on SecY and some other membrane proteins. *J. Biol. Chem.* **271,** 31196–31201 (1996).

68. Tomoyasu, T. *et al.* Escherichia coli FtsH is a membrane-bound, ATP-dependent protease which degrades the heat-shock transcription factor sigma 32. *EMBO J.* **14,** 2551–2560 (1995).

69. Langklotz, S., Baumann, U. & Narberhaus, F. Structure and function of the bacterial AAA protease FtsH. *Biochim. Biophys. Acta - Mol. Cell Res.* **1823,** 40–48 (2012).

70. Förster, A. & Hill, C. P. Proteasome Activators. *Protein Degrad.* **2,** 89–110 (2007).

71. Groll, M. *et al.* The catalytic sites of 20S proteasomes and their role in subunit maturation: A mutational and crystallographic study. *Proc. Natl. Acad. Sci.* **96,** 10976–10983 (1999).

72. Yao Huang L, Krutchinsky A, Wong ML, Standing KG, Burlingame AL, Wang CC., Y. Structural and functional characterisations of the proteasome-activating protein PA26 from Trypanosoma brucei. *J. Biol. Chem.* **274,** 33921–33930. (1999).

73. Mott, J. D. *et al.* PA28, an activator of the 20 S proteasome, is composed of two nonidentical but homologous subunits. *J. Biol. Chem.* **269,** 31466–31471 (1994).

74. Groll, M. & Huber, R. Substrate access and processing by the 20S proteasome core particle. *Int. J. Biochem. Cell Biol.* **35,** 606–616 (2003).

75. Delley, C. L., Striebel, F., Heydenreich, F. M., Özcelik, D. & Weber-Ban, E. Activity of the mycobacterial proteasomal ATPase Mpa is reversibly regulated by pupylation. *J. Biol. Chem.* **287,** 7907–7914 (2012).

76. Lander, G. C. *et al.* Complete subunit architecture of the proteasome regulatory particle. *Nature* **482,** 186–191 (2012).

77. Saeki, Y. *et al.* Ubiquitin Family Modifiers and the Proteasome. *Methods Mol. Biol.* **832,** 423–432 (2012).

78. Kupka, S., Reichert, M., Draber, P. & Walczak, H. Formation and removal of poly-ubiquitin chains in the regulation of tumor necrosis factor-induced gene activation and cell death. *FEBS J.* **283,** 2626–2639 (2016).

79. Wehmer, M. *et al.* Structural insights into the functional cycle of the ATPase module of the 26S proteasome. *Proc. Natl. Acad. Sci.* **114,** 201621129 (2017).

80. Chang, C.-Y., Hu, H.-T., Tsai, C.-H. & Wu, W.-F. The degradation of RcsA by

ClpYQ(HslUV) protease in Escherichia coli. *Microbiol. Res.* **184,** 42–50 (2016).

81. Burton, R. E., Baker, T. a & Sauer, R. T. Nucleotide-dependent substrate recognition by the AAA+ HslUV protease. *Nat. Struct. Mol. Biol.* **12,** 245–251 (2005).

82. Wu, W.-F., Zhou, Y. & Gottesman, S. Redundant in vitro proteolytic activities of Escherichia coli Lon and the ClpYQ(HslUV) protease. *J. Bacteriol.* **181,** 3587–3681 (1999).

83. Sundar, S., Baker, T. A. & Sauer, R. T. The I domain of the AAA+ HslUV protease coordinates substrate binding, ATP hydrolysis, and protein degradation. *Protein Sci.* **21,** 188–198 (2012).

84. Katayama, Y. *et al.* The two-component, ATP-dependent Clp protease of Escherichia coli. Purification, cloning, and mutational analysis of the ATP-binding component. *J. Biol. Chem.* **263,** 15226–15236 (1988).

85. Grimaud, R., Kessel, M., Beuron, F., Steven, a. C. & Maurizi, M. R. Enzymatic and Structural Similarities between theEscherichia coli ATP-dependent Proteases, ClpXP and ClpAP. *J. Biol. Chem.* **273,** 12476–12481 (1998).

86. Weber-Ban, E. U., Reid, B. G., Miranker, A. D. & Horwich, A. L. Global unfolding of a substrate protein by the Hsp100 chaperone ClpA. *Nature* **401,** 90–93 (1999).

87. Gottesman, S., Roche, E., Zhou, Y. & Sauer, R. T. The ClpXP and ClpAP proteases degrade proteins with carboxy-terminal peptide tails added by the SsrA-tagging system. *Genes Dev.* **12,** 1338–1347 (1998).

88. Hoskins, J. R., Singh, S. K., Maurizi, M. R. & Wickner, S. Protein binding and unfolding by the chaperone ClpA and degradation by the protease ClpAP. *Proc. Natl. Acad. Sci. U. S. A.* **97,** 8892–8897 (2000).

89. Lo, J. H., Baker, T. A. & Sauer, R. T. Characterization of the N-terminal repeat domain of Escherichia coli ClpA-A class I Clp/HSP100 ATPase. *Protein Sci.* **10,** 551–9 (2001).

90. Dougan, D. A., Reid, B. G., Horwich, A. L. & Bukau, B. ClpS, a substrate modulator of the ClpAP machine. *Mol. Cell* **9,** 673–683 (2002).

91. Hersch, G. L., Baker, T. a & Sauer, R. T. SspB delivery of substrates for ClpXP proteolysis probed by the design of improved degradation tags. *Proc. Natl. Acad. Sci. U. S. A.* **101,** 12136–41 (2004).

92. Dougan, D. A., Weber-Ban, E. & Bukau, B. Targeted delivery of an ssrA-tagged substrate by the adaptor protein SspB to its cognate AAA+ protein ClpX. *Mol. Cell* **12,** 373–380 (2003).

93. Bolon, D. N., Grant, R. A., Baker, T. A. & Sauer, R. T. Nucleotide-dependent substrate handoff from the SspB adaptor to the AAA+ ClpXP protease. *Mol. Cell* **16,** 343–350 (2004).

94. Martin, A., Baker, T. a & Sauer, R. T. Rebuilt AAA + motors reveal operating principles for ATP-fuelled machines. *Nature* **437,** 1115–1120 (2005).

95. Aubin-Tam, M. E., Olivares, A. O., Sauer, R. T., Baker, T. A. & Lang, M. J. Single-molecule protein unfolding and translocation by an ATP-fueled proteolytic machine. *Cell* **145,** 257–267 (2011).

96. Cordova, J. C., Das, D. K., Manning, H. W. & Lang, M. J. Combining single-molecule manipulation and single-molecule detection. *Curr. Opin. Struct. Biol.* **28,** 142–148 (2014).

97. Hersch, G. L., Burton, R. E., Bolon, D. N., Baker, T. A. & Sauer, R. T. Asymmetric interactions of ATP with the AAA+ ClpX6 unfoldase: Allosteric control of a protein machine. *Cell* **121,** 1017–1027 (2005).

98. Stinson, B. M., Baytshtok, V., Schmitz, K. R., Baker, T. A. & Sauer, R. T. Subunit asymmetry and roles of conformational switching in the hexameric AAA+ ring of ClpX. *Nat. Struct. Mol. Biol.* **22,** 411–416 (2015).

99. Flynn, J. M., Neher, S. B., Kim, Y. I., Sauer, R. T. & Baker, T. a. Proteomic discovery of cellular substrates of the ClpXP protease reveals five classes of ClpX-recognition signals. *Mol. Cell* **11,** 671–683 (2003).

100. Siddiqui, S. M., Sauer, R. T. & Baker, T. a. Role of the processing pore of the ClpX AAA+ ATPase in the recognition and engagement of specific protein substrates. *Genes Dev.* **18,** 369–374 (2004).

101. Choudhury, K., Andrews, J. T., Sen, P. K. & Sen, P. Forces on a nanoparticle in an optical trap. *Appl. Opt.* 12 (2008).

102. Lee, M. E., Baker, T. A. & Sauer, R. T. Control of substrate gating and translocation into ClpP by channel residues and ClpX binding. *J. Mol. Biol.* **399,** 707–718 (2010).

103. Schmitz, K. R., Carney, D. W., Sello, J. K. & Sauer, R. T. Crystal structure of Mycobacterium tuberculosis ClpP1P2 suggests a model for peptidase activation by AAA+ partner binding and substrate delivery. *Proc. Natl. Acad. Sci.* **111,** E4587–E4595 (2014).

104. Conlon, B. P. *et al.* Activated ClpP kills persisters and eradicates a chronic biofilm infection. *Nature* **503,** 365–370 (2013).

105. Kim, Y. I., Burton, R. E., Burton, B. M., Sauer, R. T. & Baker, T. a. Dynamics of substrate denaturation and translocation by the ClpXP degradation machine. *Mol. Cell* **5,** 639–648 (2000).

Chapter Two:

Highly dynamic interactions maintain kinetic stability of the ClpXP

protease during the ATP-fueled mechanical cycle

KRS developed kinetic fitting models for data analysis. I collected all data shown and developed the BLI approach described.

ABSTRACT

The ClpXP protease assembles in a reaction in which an ATP-bound ring hexamer of ClpX binds to one or both heptameric rings of the ClpP peptidase. Contacts between ClpX IGF-loops and clefts on a ClpP ring stabilize the complex. How ClpXP stability is maintained during the ATP-hydrolysis cycle that powers mechanical unfolding and translocation of protein substrates is poorly understood. Here, we use a real-time kinetic assay to monitor the effects of nucleotides on the assembly and disassembly of ClpXP. When ATP is present, complexes containing single-chain ClpX assemble via an intermediate and remain intact until transferred into buffers containing ADP or no nucleotide. ATP binding to high-affinity subunits of the ClpX hexamer prevents rapid dissociation but additional subunits must be occupied to promote assembly. Small-molecule acyldepsipeptides, which compete with the IGF loops of ClpX for ClpP-cleft binding, cause exceptionally rapid dissociation of otherwise stable ClpXP complexes, suggesting that the IGF-loop interactions with ClpP must be highly dynamic. Our results indicate that the ClpX hexamer spends almost no time in an ATP-free state during the ATPase cycle, allowing highly processive degradation of protein substrates.

INTRODUCTION

The ATP-powered ClpXP protease consists of the AAA+ ClpX hexamer and the ClpP peptidase, which contains two heptameric rings.[1] ClpX can bind one or both heptameric faces of ClpP, recognizes specific protein substrates via ssrA tags or other peptide degrons, and uses the energy of ATP hydrolysis to unfold and translocate substrates through an axial channel and into the degradation chamber of ClpP (Figure 2.1a). ClpX binding to ClpP requires ATP or ATPγS, a slowly hydrolyzed ATP analog, but is not observed in the absence of nucleotide or in the presence of ADP.[2-5] However, the role of ATP in stabilizing ClpXP complexes is poorly characterized. Moreover, the kinetics of ClpXP assembly and disassembly have not been carefully studied, in part because established binding assays rely on changes in ClpX or ClpP activity, require the continual presence of ATP/ATPγS, and/or are poorly suited for measuring rapid changes in assembly state.

ClpX hexamers dissociate at low concentrations, an event that is also nucleotide dependent,[2] potentially complicating studies of ClpP binding. However, ClpX subunits lacking the N domain (ClpX$^{\Delta N}$) can be linked using genetically encoded tethers, and single-chain ClpX$^{\Delta N}$ pseudohexamers retain wild-type levels of mechanical activity, as shown by their ability to collaborate with ClpP in degradation of ssrA-tagged substrates.[6] Pseudohexamer variants have been used to assess the number of active subunits needed for function, to show that mechanical activity requires subunit switching from ATP-binding to non-binding conformations, to establish that pore loops cooperatively grip substrates, to determine subunit-specific ATP affinities, and to visualize single-molecule unfolding and translocation in optical-trapping experiments.[6-15]

Most stabilization of ClpXP complexes arises from contacts between hydrophobic clefts on the periphery of the heptameric ClpP ring and flexible loops in the ClpX hexamer that contain an IGF or related tripeptide sequence (Figure 2.1a,b).[5,16–18] Contacts between axial pore-2 loops in ClpX and stem-loop structures in ClpP also contribute to ClpXP stability,[16] but elimination of these axial interactions impairs binding less than deletion of a single IGF loop from the ClpX hexamer.[16] Interestingly, small-molecule acyldepsipeptides, such as ADEP-2B, also bind to the ClpP clefts, mimicking IGF-loop binding (Figure 2.1c).[19–21] ADEPs have antibacterial activity because they open the axial ClpP pore, causing indiscriminate degradation of unstructured proteins.[22–23]

Fiber-optic biosensors and bio-layer interferometry (BLI) can be used for real-time assays of macromolecular interactions, as the signal is sensitive to changes in mass on the biosensor surface.[24] Here, we use this method to examine how nucleotides and ADEPs affect the kinetics of ClpP binding to single-chain ClpX pseudohexamers, eliminating potential complications caused by hexamer dissociation. Our results show that the ATP requirements for assembly and maintenance of complex stability differ, suggest that IGF-loop interactions with ClpP are highly dynamic under conditions where the complex is extremely stable, and support a model in which the ClpX hexamer spends very little time in an ATP-free state, facilitating highly processive protein degradation.
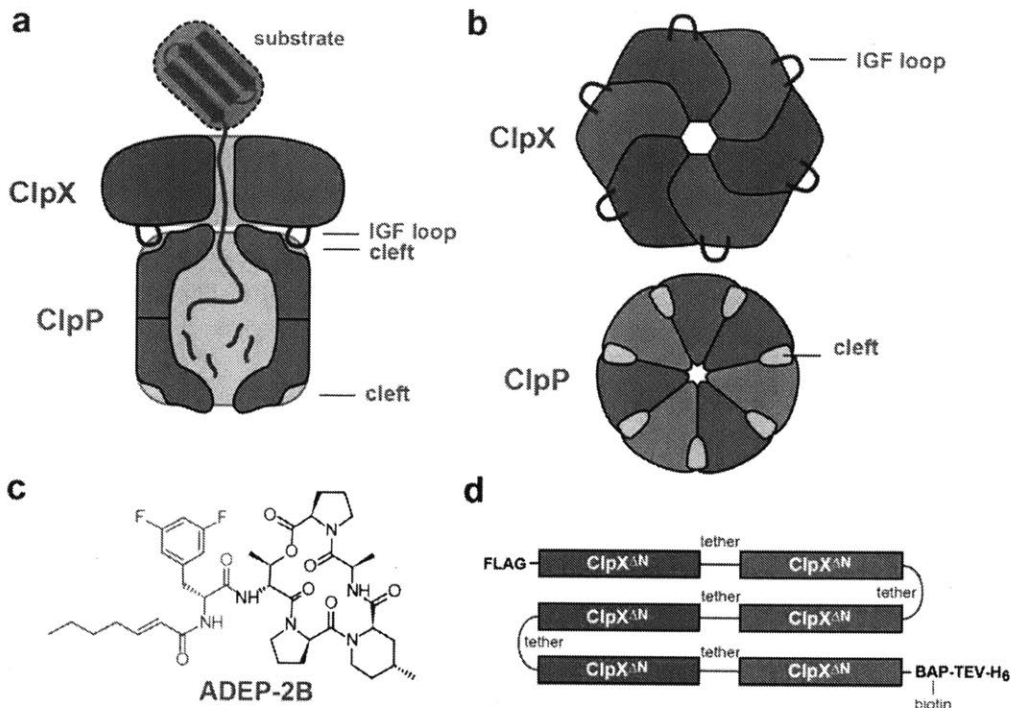
Figure 2.1. The ClpXP protease. **a**) Side view of ClpXP degrading a substrate (green). A ClpX hexamer (blue) recognizes, unfolds, and translocates protein substrates into the degradation chamber of ClpP (dark orange), which consists of two heptameric rings. ClpXP is principally stabilized by interactions between the IGF loops of ClpX and hydrophobic clefts on each ClpP ring. **b**) Axial view of a ClpX homohexameric ring and a ClpP homoheptameric ring, highlighting the interaction elements. **c**) Chemical structure of ADEP-2B.[21,28] The portion thought to mimic binding of an IGF tripeptide is colored purple. **d**) ^{sc6}ClpX$^{\Delta N}$-bio is a single-chain pseudohexamer in which the ClpX$^{\Delta N}$ subunits are linked by six-residue tethers. The protein contains an N-terminal FLAG tag and a C-terminal sequence consisting of a biotin acceptor peptide (BAP), a cleavage site for Tobacco Etch Virus protease (TEV), and six histidines (H$_6$).

RESULTS AND DISCUSSION

Assembly requires ATP binding. We used BLI to probe binding of an *Escherichia coli* ClpP variant to a ClpX pseudohexamer immobilized on a streptavidin-coated biosensor. The pseudohexamer consisted of *E. coli* ClpX$^{\Delta N}$ subunits covalently connected by six-residue peptide tethers with a biotin near the C-terminus (^{sc6}ClpX$^{\Delta N}$-bio; Figure 2.1d). Single-chain ClpX$^{\Delta N}$ supports ClpP-dependent degradation of ssrA-tagged protein substrates in solution and when

immobilized to a streptavidin surface.[6,7,10–15,25,26] In a typical BLI experiment, the biosensor was sequentially loaded with ^{sc6}ClpX$^{\Delta N}$-bio, transferred into ATP, moved into ATP and ClpP to allow binding, and finally transferred into ClpP-free buffer with ATP to allow dissociation (Figure 2.2a). In this experiment, ClpP binding to ^{sc6}ClpX$^{\Delta N}$-bio saturated after ~30 s, but no dissociation was observed over several minutes. ClpP bound to ^{sc6}ClpX$^{\Delta N}$-bio with similar kinetics in the presence of ATP or ATPγS (Figure 2.2b). Because ClpX hydrolyzes ATP ~20-times faster than ATPγS,[4] binding of these nucleotides rather than their hydrolysis rates must determine the ClpXP assembly rate. ClpP did not bind ^{sc6}ClpX$^{\Delta N}$-bio in the presence of ADP or without nucleotide (Figure 2.2b).

We performed association experiments using ATP and different ClpP concentrations. Binding trajectories at low ClpP concentrations fit well to a single exponential, as expected for a pseudo first-order reaction, whereas a double exponential was needed to fit trajectories for ClpP concentrations ≥ 500 nM (see Figure 2.2c for examples). For ClpP concentrations ≤ 200 nM, the rate constants (k_{obs}) from single-exponential fits varied linearly with ClpP concentration (Figure 2.2d), with a slope that corresponds to the association rate constant ($6.6 \cdot 10^5$ M^{-1}s^{-1}). The two rate constants from the double-exponential fits varied in a hyperbolic fashion between 0.5 and 20 μM ClpP (Figure 2.2e), suggesting that a unimolecular reaction becomes rate-limiting in ClpXP assembly at high ClpP concentrations. The shift from single- to double-exponential assembly kinetics at high ClpP concentrations is consistent with a model in which ClpX species with different ClpP-binding properties interconvert.
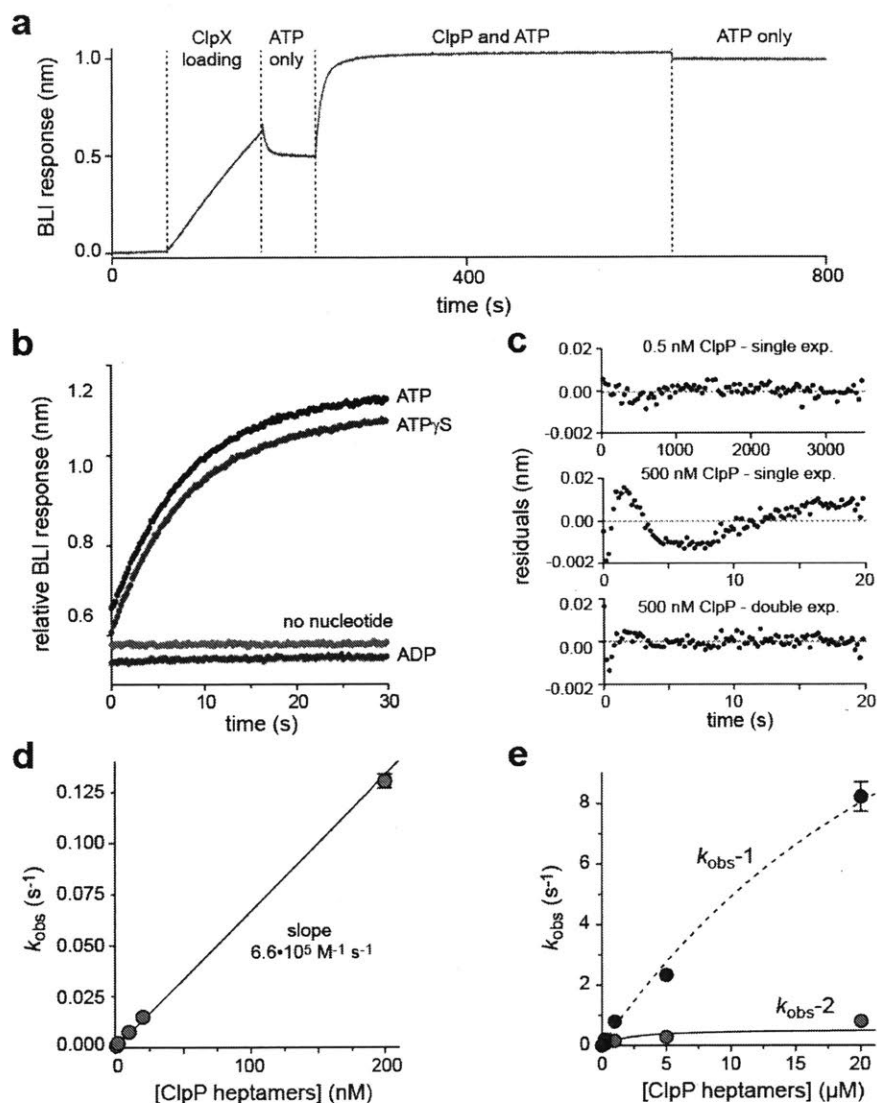
Figure 2.2. Association of ClpP with ^{sc6}ClpX$^{\Delta N}$-bio assayed by BLI. **a**) A streptavidin-coated BLI biosensor was incubated sequentially with buffer, buffer plus 20 nM ^{sc6}ClpX$^{\Delta N}$-bio, buffer plus 2 mM ATP, buffer plus 200 nM ClpP and 2 mM ATP, and buffer plus 2 mM ATP. **b**) BLI trajectories showing that ClpP binding to ^{sc6}ClpX$^{\Delta N}$-bio occurs with similar kinetics in the presence of ATP or ATPγS (2 mM each). Binding was not observed with 2 mM ADP or no nucleotide. Individual trajectories are offset to allow comparisons. **c**) Residuals of single-exponential and/or double-exponential fits for association trajectories obtained using ClpP concentrations of 0.5 or 500 nM. **d**) For ClpP concentrations of 200 nM or less, rate constants from single-exponential fits of ClpP association trajectories (k_{obs}) varied linearly with ClpP, with a slope corresponding to the second-order association rate constant. **e**) Variation of the rate constants from double-exponential fits for ClpP concentrations of 500 nM or higher. The curves

are fits to a hyperbolic equation. For k_{obs}-1 (amplitude ~70%), the maximal rate was 22 ± 7 s^{-1} with a half-maximal concentration of ~35 μM ClpP heptamer. For k_{obs}-2 (amplitude ~30%), the maximal rate was 0.54 ± 0.2 s^{-1} with a half-maximal concentration of ~2 μM ClpP heptamer.

We measured binding of 200 nM ClpP to ^{sc6}ClpX$^{\Delta N}$-bio at different ATP concentrations, determined k_{obs}, plotted normalized values against [ATP], and fit these data to the Hill equation (Figure 2.3a). Assembly proceeded at half the maximal rate at an ATP concentration of ~100 μM with a Hill constant (n) of 2.1. The steady-state rate of ATP hydrolysis in the absence of ClpP was half-maximal at an ATP concentration of 42 μM (V_{max} = 73 min^{-1} enz^{-1}; n = 2.4). Thus, ~2-fold higher ATP is required for half-maximal association than for half-maximal hydrolysis (Figure 2.3a). This result could mean that an additional molecule of ATP must bind to a hydrolytically active ClpX hexamer to promote ClpP binding. Alternatively, ClpP-binding and non-binding subpopulations of ClpX hexamers may equilibrate, with the binding conformation having slightly weaker affinity for ATP. This model seems less likely, as K_M for ATP hydrolysis by ^{sc6}ClpX$^{\Delta N}$-bio in the presence of excess ClpP was 29 μM (V_{max} = 41 min^{-1} enz^{-1}; n = 2.2), in agreement with studies showing that ClpP reduces K_M for wild-type ClpX.[4]
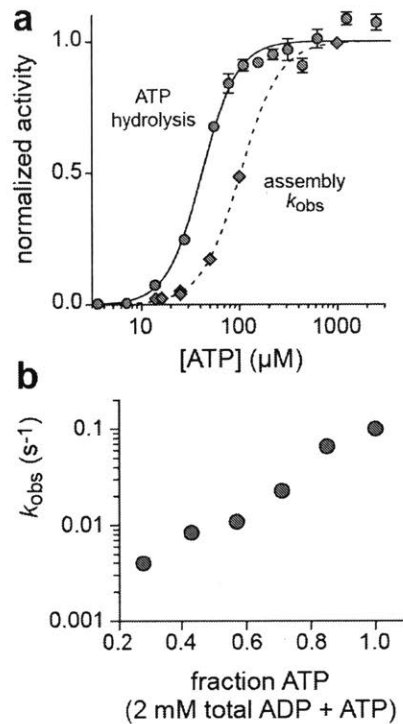
Figure 2.3. Nucleotide dependence of ClpP association. **a)** Graphs showing normalized $^{sc6}ClpX^{\Delta N}$-bio ATP-hydrolysis activity and normalized ClpP association rate constants (obtained using 200 nM ClpP) as a function of ATP concentration. The curves are fits to a Hill equation (Y = $[ATP]^n/(K_{app}^n + [ATP]^n)$). For ATP hydrolysis, the fitted values of K_{app} and n were 42 ± 3 μM and 2.4 ± 0.3, respectively. For assembly, these fitted values were 100 ± 2 μM and 2.1 ± 0.06, respectively. Maximal fitted values prior to normalization were 73 ± 1 min^{-1} enz^{-1} for ATP hydrolysis and 0.138 ± 0.001 s^{-1} for k_{obs}. **b)** Variation of k_{obs} for 200 nM ClpP association with the fraction of ATP in mixtures with ADP (2 mM total nucleotide).

We measured k_{obs} values for association of 200 nM ClpP in different concentrations of ATP and ADP that totaled 2 mM (Figure 2.3b). As the ADP concentration increased and ATP concentration decreased, the association rate slowed appreciably. For example, 0.5 mM ATP plus 1.5 mM ADP supported ClpXP binding, but at a rate ~25-fold slower than observed with 2 mM ATP. This decrease in the association rate in the presence of excess ADP probably reflects

reduced ATP binding, as a result of competitive inhibition, and increased ADP occupancy of ClpX subunits.[8]

Nucleotide dependence of dissociation. To test if ClpXP complexes require the continued presence of nucleotide, we bound ClpP to immobilized $^{sc6}ClpX^{\Delta N}$-bio in the presence of ATP and transferred the biosensor into ClpP-free buffer containing ADP, ATP, or ATPγS. ClpXP complexes dissociated with a half-life of ~5 s in the presence of ADP but remained stable in ATP or ATPγS (Figure 2.4a). GFP-ssrA, a good protein substrate, did not prevent rapid dissociation when ClpXP was transferred from ATP into ADP (not shown). For complexes formed with ATPγS, the half-life after transfer into ClpP-free buffer containing ADP was ~20 s, (Figure 2.4b). As ClpX hydrolyzes ATP more rapidly than ATPγS,[4] loss of ATP through faster hydrolysis appears to result in faster ClpP dissociation. Indeed, after transfer into nucleotide-free buffer, ATP-stabilized ClpXP dissociated ~50-times faster than ATPγS-stabilized ClpXP or an ATP-stabilized ClpXP complex containing ATPase-defective REEREE ClpX (Figure 2.4c). The REEREE complex dissociated with similar kinetics in buffers containing no nucleotide or ADP (not shown). By contrast, ATPγS-stabilized ClpXP was more stable in nucleotide-free buffer (Figure 2.4c) than in buffer containing ADP (Figure 2.4b), suggesting that ADP binding to unoccupied ClpX subunits stimulates ATPγS hydrolysis or release.

These results show that ClpX-bound ATP or ATPγS that leaves by dissociation or hydrolysis must be replaced to maintain stable ClpXP complexes. When we transferred ATP-stabilized complexes into ClpP-free buffer with different concentrations of ATP, rapid dissociation was only observed at ATP concentrations of 10 µM or less (Figure 2.4d). As half-maximal assembly

required 20-fold higher ATP concentrations, occupancy of a subset of high-affinity ClpX sites appears to be sufficient to maintain a kinetically stable complex. This result is consistent with experiments that show that different subunits in the ClpX hexamer bind ATP with a range of affinities.[8] ClpXP complexes transferred into buffer with a 7:1 mixture of ADP:ATP (2 mM total) were ~100-fold more kinetically stable than those transferred into ADP alone (Figure 2.4e), suggesting that complexes containing a mixture of ADP-bound and ATP-bound ClpX subunits are quite stable.

In ClpP-free buffer containing 2 mM ATP, little dissociation of ClpXP complexes was observed over 1000 s when the biosensor was washed twice with fresh buffer, moved into buffer containing non-biotinylated ^{sc6}ClpX$^{\Delta N}$ to prevent rebinding of dissociated ClpP, or transferred into buffer containing the GFP-ssrA substrate (Figure 2.4f). Substantially longer BLI experiments were not possible because of sample evaporation. Assuming that fewer than 5% of ClpXP complexes dissociate in 15 min, the upper limit for the dissociation rate constant is ~$6 \cdot 10^{-5}$ s^{-1}. Based on this value and an association rate constant of $6.6 \cdot 10^5$ M^{-1}s^{-1}, an affinity of ~100 pM or tighter would be predicted for ClpP binding to ^{sc6}ClpX$^{\Delta N}$-bio. We were unable to obtain reliable equilibrium response values at sub-nM ClpP concentrations. A hyperbolic fit of the equilibrium BLI response versus total ClpP from 1-20 nM predicted half-maximal binding at ~160 ± 75 pM (Figure 2.4g), although the absence of data below 80% binding make the fit unreliable. Moreover, the fitted half-maximal value is an upper bound because the amount of ^{sc6}ClpX$^{\Delta N}$-bio bound to the biosensor and thus the free ClpP concentration at half-maximal binding are unknown.
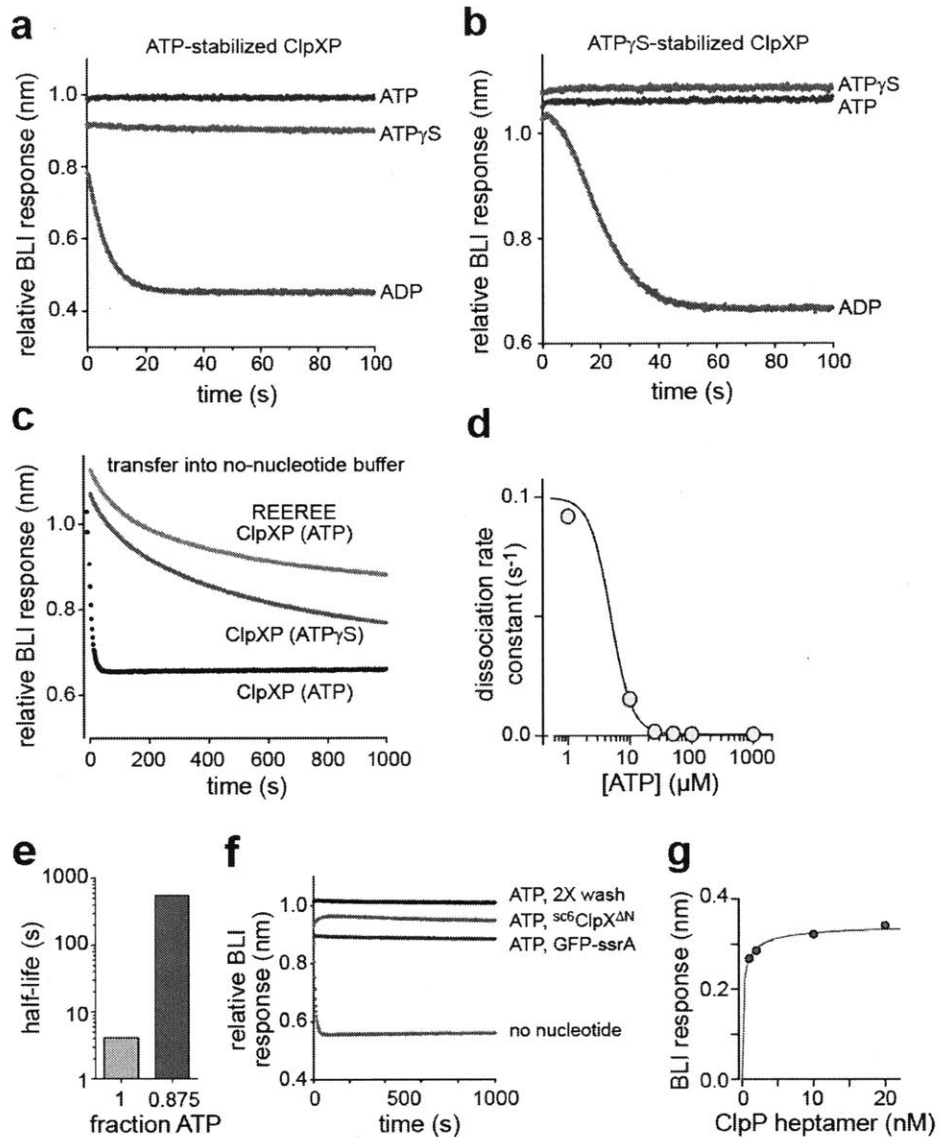
Figure 2.4. Dissociation and equilibrium stability of ClpXP complexes. **a**) Complexes were assembled with ^{sc6}ClpX$^{\Delta N}$-bio bound to the biosensor, 200 nM ClpP, and 2 mM ATP. At time zero, the biosensor was moved into ClpP-free buffer containing 2 mM ADP, 2 mM ATP, or 2 mM ATPγS. The trajectories have been offset vertically, but all start at the same BLI value ± 5%. **b**) The same experiment as shown in panel A, except ClpXP complexes were assembled in the presence of 2 mM ATPγS. **c**) Dissociation kinetics after transfer into buffer without nucleotide for ClpP complexes assembled with ATPase-active ^{sc6}ClpX$^{\Delta N}$-bio and ATP (bottom curve), ATPase-active ^{sc6}ClpX$^{\Delta N}$-bio and ATPγS (middle curve) or a ATP-hydrolysis defective REEREE ^{sc6}ClpX$^{\Delta N}$-bio variant and ATP (top curve). **d**) Complexes were assembled with ATP as in panel **a** and then transferred into ClpP-free buffer containing different concentrations of

ATP. Dissociation rate constants were calculated from single-exponential fits and plotted as a function of the ATP concentration. The line is a fit to the Hill equation. e) Half-lives of ClpXP complexes assembled in ATP following transfer into buffer containing 100% ADP (2 mM) or 87.5% ADP (1.75 mM ADP; 0.25 mM ATP). (f) BLI trajectories showing that ClpXP complexes are stable for long periods in ClpP-free buffer containing 2 mM ATP, 2 mM ATP and unbiotinylated ^{sc6}ClpX$^{\Delta N}$ (1 µM), or 2 mM ATP and GFP-ssrA (20 µM). g) Equilibrium BLI response for ^{sc6}ClpX$^{\Delta N}$-bio binding as a function of total ClpP concentration. The fitted curve is a hyperbolic equation with half-maximal binding at a total ClpP concentration of 160 ± 75 pM.

ADEP-induced dissociation. ADEPs bind to the same ClpP clefts as the IGF loops of ClpX.[19-21]

Notably, even in the presence of ATP, addition of 50 µM ADEP-2B caused extremely rapid

dissociation of ClpXP complexes (Figure 2.5a), ruling out a strictly competitive model in which

ADEPs simply prevent ClpX rebinding following spontaneous dissociation. Instead, ADEP-2B

must bind to the ClpXP complex and actively promote ClpX dissociation, possibly by a

mechanism that involves transient unbinding of an IGF loop from a ClpP cleft and filling of this

cleft by ADEP. ADEP-induced dissociation (~1 s half-life) was faster than ADP-induced

dissociation (~5 s half-life), and 200 nM ADEP-2B promoted similar rates of dissociation for

ATP-stabilized and ATPγS-stabilized ClpXP complexes (Figure 2.5b), indicating that ATP

hydrolysis is not required for ADEP-induced dissociation effect.

ClpXP dissociation rates determined at different ADEP-2B concentrations fit well ($R^2 = 0.994$)

to a hyperbolic equation expected if binding of just one ADEP-2B molecule to an appropriate

ClpP site causes ClpX dissociation (Figure 2.5c). By contrast, mechanisms requiring binding of

two or three ADEP-2Bs to identical and independent ClpP sites predict sigmoidal curves that fit

more poorly (see Figure 2.5c legend). Strikingly, ~50 µM ADEP-2B was required for 50%

stimulation of ClpXP dissociation (Figure 2.5c), whereas ~200 nM ADEP-2B resulted in 50%

stimulation of decapeptide cleavage by ClpP alone or 50% inhibition of ClpXP assembly (Figure

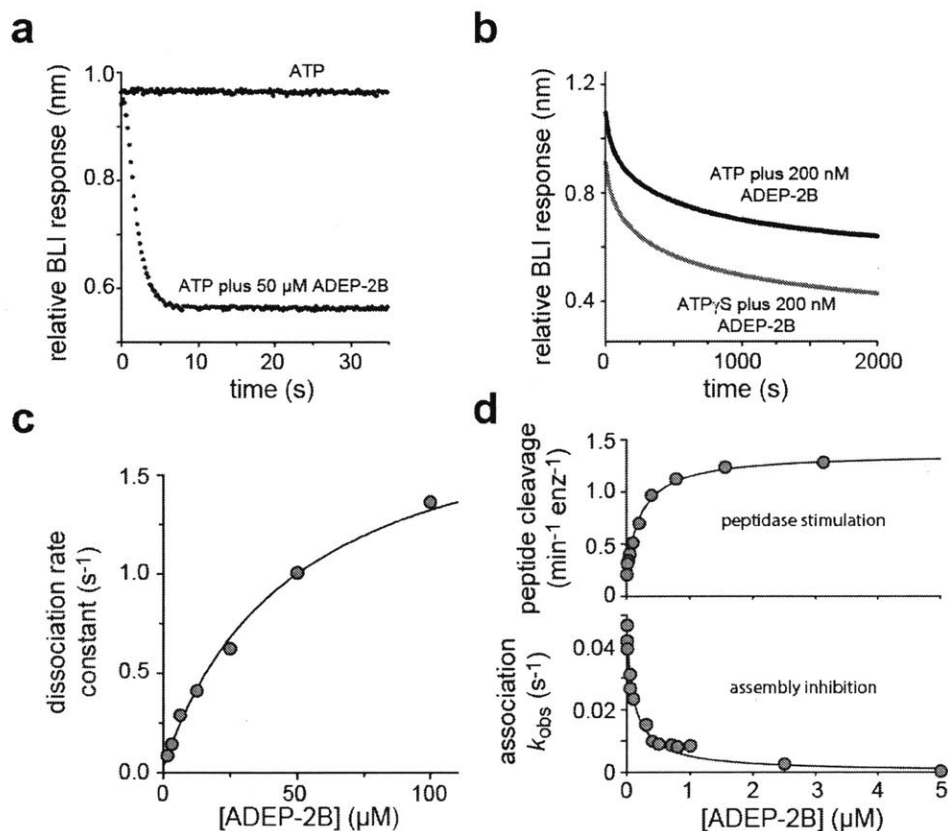2.5d). As discussed below, these results support a dynamic-competition model for ADEP-induced dissociation.

Figure 2.5. ADEP effects. **a**) BLI trajectories following transfer of ATP-stabilized ClpXP into ClpP-free buffer containing 2 mM ATP without or with 50 μM ADEP-2B. **b**) BLI trajectories following transfer of ATP-stabilized ClpXP into ClpP-free buffer containing 200 nM ADEP-2B and 2 mM ATP or ATPγS. **c**) ADEP-2B stimulation of dissociation. ATP-stabilized ClpXP was transferred into ClpP-free buffer containing 2 mM ATP and different ADEP-2B concentrations, and dissociation rate constants were determined by single-exponential fits. The line is a hyperbolic fit ($R^2 = 0.994$) with values of 2.0 ± 0.13 s^{-1} for the maximum rate and 50 ± 7 μM for half-maximal stimulation. Sigmoidal equations for mechanisms involving two ADEPs ($\alpha^2/(1+2\alpha+\alpha^2)$; $\alpha = $ [ADEP]$/K_\mu$; $R^2 = 0.971$) or three ADEPs ($\alpha^3/(1+3\alpha+3\alpha^2+\alpha^3)$; $R^2 = 0.958$) gave poorer fits. **d**) (top) ADEP-2B stimulation of decapeptide cleavage of 25 nM ClpP. The line is a hyperbolic fit ($R^2 = 0.995$) with half-maximal inhibition at a total concentration of 240 ± 26 nM. (bottom) ADEP-2B inhibition of association of 200 nM ClpP. The line is a hyperbolic fit ($R^2 = 0.981$) with half-maximal inhibition at a total concentration of 167 ± 20 nM.

Stepwise assembly. Our results show that the ClpXP assembly rate increases linearly with low concentrations of ClpP, as expected for a bimolecular reaction,. However, this rate saturates at high ClpP concentrations, supporting a model in which the rate-limiting step switches from a bimolecular to a unimolecular reaction. For example, single-chain ClpX could initially collide with ClpP to form an unstable intermediate in which only one or a few IGF loops in the ClpX hexamer interact with ClpP, with docking of the remaining loops becoming the rate-limiting unimolecular step in formation of the stable complex at high ClpP concentrations. Following assembly, however, ClpXP complexes are extremely stable in buffers containing ATP, unless ADEPs are also present. It is possible that these aspects of assembly and disassembly might not apply to unlinked ClpXP complexes or be observed using assays other than BLI. For example, unlinked ClpXP might be less kinetically stable because of ClpX hexamer dissociation, or association might be strictly second-order if ClpX was not surface bound.

Dynamic IGF-cleft interactions. ADEP, a small-molecule antibiotic, binds in the same ClpP clefts as the IGF loops of ClpX, and ADEP or ClpX binding opens the axial pore of ClpP.[17,19–21,27] Based on these observations, we anticipated that ADEPs would be competitive inhibitors of ClpX binding to ClpP. However, a strictly competitive model requires dissociation of ClpXP complexes before ADEPs can bind and prevent reassociation. By contrast, we find that high ADEP-2B concentrations reduce the ClpXP half-life to ~1 s, accelerating dissociation by more than 10^4-fold. Moreover, the concentration dependence of ADEP-2B-induced ClpXP dissociation suggests that binding of a single ADEP to the ClpXP complex is sufficient to drive dissociation. In principle, ADEP binding to an empty cleft on the ClpP ring might drive an allosteric conformational change that results in ClpXP dissociation (Figure 2.6a). However, based on differences in affinity, the free energy of ClpP binding by our single-chain ClpX

hexamer is far more favorable than ADEP-2B binding.[28] Thus, it is unlikely that one ADEP-binding event would be thermodynamically capable of driving the ClpXP complex into a conformation that forces rapid ClpX dissociation.

Our results support a "dynamic competition" model in which one ClpX IGF loop transiently unbinds a ClpP cleft, allowing an ADEP to bind and accelerate dissociation by preventing rebinding of the undocked loop (Figure 2.6b). By this model, ADEP binding to ClpP clefts that are not needed for IGF binding would not promote ClpXP disassembly and thus be "invisible" in terms of the concentration dependence of dissociation. Deletion of a single IGF loop from the ClpX hexamer impairs ClpP binding modestly.[16] Moreover, in a hexamer with six loops, steric clashes between a transiently unbound loop and a bound ADEP could dramatically destabilize the complex. In the ClpXP complex, the ADEP-binding sites that could drive ClpX dissociation would normally be inaccessible because they are occupied by IGF loops. Thus, compared to open clefts, high ADEP concentrations would be required to bind these transiently unoccupied sites. Consistently, half-maximal ADEP-2B concentrations required to accelerate ClpXP dissociation were ~250-fold higher than those required to inhibit assembly or stimulate ClpP-pore opening. Isolated IGF peptides bind weakly to ClpP,[27] and thus transient unbinding of an IGF loop in the complex should have a low energy barrier. Despite the dynamic nature of these interactions, tight overall binding presumably arises because the six contacts are mutually stabilizing and the high effective concentration of IGF loops with respect to ClpP clefts favors rebinding of any undocked loop as a consequence of the small entropic cost.

Additional mechanistic implications. IGF-loop flexibility was initially proposed to allow ClpXP docking despite the symmetry mismatch between six loops in the ClpX hexamer and

seven clefts in a ClpP ring.[17] Consistent with some flexibility, the IGF loops are proteolytically accessible in free ClpX and disordered in crystal structures of ClpX ring hexamers.[7,18,29] If these loops are truly flexible, however, then why is ATP or ATPγS required for detectable binding of ClpX to ClpP? ATP binding might stabilize an IGF-loop conformation that allows it to dock efficiently with ClpP (Figure 2.6c). Alternatively, ATP binding might affect the geometry with which the six IGF loops are arranged with respect to the clefts on the ClpP ring (Figure 2.6d), with only some IGF loops in ADP-bound or nucleotide-free ClpX able to engage ClpP clefts.
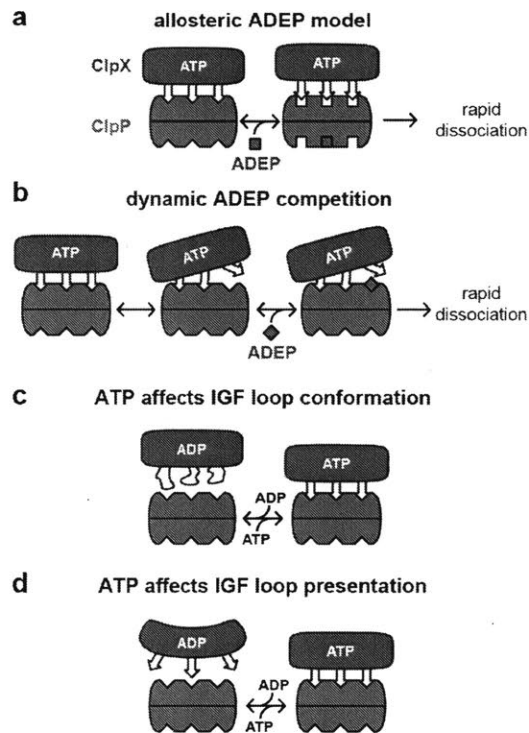
Figure 2.6. Models for small-molecule control of complex stability. **a)** ADEP binding to an empty ClpP cleft allosterically stabilizes a conformation from which ClpX rapidly dissociates. For simplicity, only a subset of IGF loops in ClpX and clefts in each ring of ClpP are shown. **b)** ADEP binding to a ClpP cleft transiently unoccupied by an IGF loop prevents re-docking and stimulates dissociation. **c)** ATP binding to the ClpX hexamer stabilizes a conformation of the IGF loops that binds the ClpP clefts more efficiently. **d)** ATP binding to the ClpX hexamer positions the IGF loops to interact optimally with ClpP.

Although each subunit of ClpX has the same sequence, conformational changes create an asymmetric hexamer consisting of some subunits that cannot bind nucleotide and others that bind ATP/ADP with a range of affinities.[7,8,29,30] We find that half-maximal activation of ClpP binding by ^{sc6}ClpX$^{\Delta N}$-bio requires higher ATP concentrations than half-maximal activation of ATP hydrolysis, making it likely that more ClpX subunits need to be ATP bound for ClpP binding than for ATP hydrolysis. However, concentrations of ATP that support less than 5% of the maximal ATP-hydrolysis activity can maintain substantial kinetic stability of preformed ClpXP complexes, indicating that occupancy of just high-affinity ClpX subunits suffices for this activity. ClpX hexamers containing a mixture of ATP-bound and ADP-bound subunits also bind ClpP with substantial kinetic stability relative to the rate of ATP hydrolysis.

ClpX does not hydrolyze ATP using a concerted or strictly sequential mechanism,[6] but optical-trapping experiments suggest that kinetic bursts of ATP hydrolysis in multiple subunits power substrate translocation.[12,13] One model to explain these bursts posits that all bound ATP is hydrolyzed rapidly with subsequent fast release of P$_i$ and ADP, followed by slow rebinding of ATP.[12] This model predicts that ClpX would frequently be nucleotide-free or have only ADP-bound subunits. Our results allow estimation of an upper limit for the fraction of time that ClpXP spends in a nucleotide-free or ADP-bound state (f) during the normal ATPase cycle. Specifically, the ClpP dissociation rate constant in the absence of nucleotide or presence of ADP (< 0.07 s^{-1}) multiplied by f must be less than the dissociation rate constant in the presence of ATP (< 0.00006 s^{-1}). Thus, f must be less than 0.0008. Hence, under the conditions of our experiments, ClpXP appears to spend a very small fraction of time in an all ADP-bound or nucleotide-free state. ClpX

hydrolyzes ATP at a rate of ~(1 s^{-1})•[ClpX] at ATP concentrations of 10^{-3} M or higher. If ClpX

passed through a nucleotide-free state during each ATPase cycle, then the rate of ATP binding

(k_a•[ATP][nucleotide-free ClpX]) would be less than (0.01 s^{-1})•[ClpX] based on a k_a value of

1.3•10^4 M^{-1}s^{-1},[4] an ATP concentration of 10^{-3} M, and a nucleotide-free ClpX concentration of

[f•ClpX]. Because the steady-state rate of ATP hydrolysis cannot be 100-fold faster than the rate

of ATP binding, we conclude that a nucleotide-free state cannot be an obligatory or even

common intermediate in the ATPase cycle. As a consequence, we propose that at least one

subunit in the ClpX hexamer remains ATP-bound during the normal ATPase cycle, with the

remaining subunits being ATP-bound, ADP-bound, or nucleotide-free depending on progress

through the cycle. This mechanism would preserve ClpP binding and maintain grip on the

polypeptide substrate, which is also ATP dependent.[31]

The degron of a protein substrate is degraded soon after it enters the proteolytic chamber of

ClpP. If ClpXP dissociated after this event, then the remaining substrate would be released.

However, with a few notable exceptions, degradation by ClpXP is highly processive even though

hundreds of ATP-hydrolysis events can be required to degrade a single protein substrate.[9,32–34]

This degree of high processivity is likely to occur because ClpXP complexes rarely dissociate, as

they spend almost no time in an ATP-free state.

AAA+ proteolytic machines. The proteolytic complexes of other AAA+ proteases – including

ClpAP, ClpCP, HslUV, Cdc48•20S, PAN•20S, Mpa•20S, and the 26S proteasome – are also

stabilized in an ATP-dependent fashion by contacts between peripheral peptide or loop elements

from each subunit of a AAA+ unfolding ring and clefts or grooves on the corresponding self-

compartmentalized peptidase ring.[35] Except for HslUV, the assembly of all of these machines

also involve a symmetry mismatch between a hexameric AAA+ unfolding ring and a heptameric protease ring. The functional significance of these mismatches is unknown and may simply represent random evolutionary solutions that worked. All AAA+ proteolytic machines must cycle through a variety of nucleotide-dependent conformations as they mechanically unfold and translocate protein substrates. As a consequence, we suspect that the interactions that stabilize these proteolytic machines will also be highly dynamic and influence their mechanisms of assembly and disassembly. Consistently, assembly chaperones for the 26S proteasomal base, which includes the Rpt_{1-6} AAA+ ring, can drive its dissociation from the 20S peptidase.[36]

METHODS

Proteins. The $^{sc6}ClpX^{\Delta N}$-bio pseudohexamer was expressed from plasmid pACYC and contained an N-terminal FLAG tag (MADYKDDDDKHM); six *E. coli* $ClpX^{\Delta N}$ subunits (with C169S and K408E substitutions) connected by the sequences GGGTSG, GGTSSG, GGSSSG, GGSAGS, and GGGSSG, respectively; an AAAGLNDIFEAQKIEWH biotin acceptor peptide;[37] and a TEV-H_6 tag (ENLYFQSHHHHHH) at the C-terminus. As judged by the fraction of purified protein that bound to streptavidin, ~50% of the ClpX pseudohexamer was biotinylated *in vivo*. To prevent ATP hydrolysis, the REEREE $^{sc6}ClpX^{\Delta N}$-bio variant contained the R270K sensor-II mutation in subunits 1 and 4 and the E185Q Walker-B mutation in subunits 2, 3, 5, and 6.[5,6,30] *E. coli* ClpP was expressed from pET-22b (EMD Millipore), contained the C91V and C113A substitutions, and had a TEV-His_6 tag at the C-terminus. Both $^{sc6}ClpX^{\Delta N}$-bio and ClpP were purified from *E. coli* ER2566 cells (New England Biolabs) transformed with plasmids containing the appropriate gene under T7-promoter control. Cells were initially grown to an OD_{600} of ~0.7 at 37 °C in media containing 13 g L^{-1} peptone, 7.5 g L^{-1} yeast extract, and 5 g L^{-1} NaCl. At this time, 1 mM isopropyl β-D-1-thiogalactopyranoside (Teknova) was added and growth was

continued for 4 h at room temperature. Harvested cells were resuspended in lysis buffer (20 mM

HEPES, pH 7.5, 400 mM NaCl, 100 mM KCl, 20 mM imidazole, and 10% glycerol (v/v)), lysed

by sonication, centrifuged at 12,000 rpm in a Sorvall SA-600 rotor, and the supernatant was

incubated with Ni-NTA agarose beads (Thermo Fisher Scientific) for 1 h. The beads were

transferred to a gravity column, washed with 5 volumes of lysis buffer, and ^{sc6}ClpX$^{\Delta N}$-bio or

ClpP protein was eluted with five 1-mL aliquots of lysis buffer plus 300 mM imidazole.

Fractions containing protein were pooled and desalted into column buffer (25 mM HEPES, pH

7.5, 50 mM KCl, 10% glycerol) using a PD-10 column (GE Healthcare). Both proteins were

further purified by MonoQ ion-exchange chromatography and Superdex-200 gel-filtration

chromatography (GE Healthcare) as described.[16] Prior to Mono-Q, the H$_6$ tag on the ClpP-TEV-

H$_6$ construct was removed by digestion with TEV protease, followed by passage through Ni-

NTA agarose to remove any H$_6$-tagged protein. Superdex-200 fractions containing purified

^{sc6}ClpX$^{\Delta N}$-bio or ClpP were pooled and stored frozen at –80 °C. ^{sc6}ClpX$^{\Delta N}$-bio concentrations

were calculated for the pseudohexamer; ClpP concentrations were calculated in heptamer

equivalents, the unit that binds a ClpX hexamer.

Assays. Assays were performed at 30 °C in a buffer containing 25 mM HEPES (pH 7.5), 100

mM KCl, 10 mM MgCl$_2$, 10% glycerol, 0.05% TWEEN-20 (EMD Millipore), supplemented as

necessary with ATP (Sigma-Aldrich), ATPγS (Roche), or ADP (Sigma-Aldrich). ADEP-2B was

synthesized as described,[28] and experiments using it contained 5% (v/v) dimethylsulfoxide (Alfa

Aesar), which decreased the ClpXP association rate ~3-fold. BLI experiments were performed

using an Octet RED96 instrument (ForteBio), 96-well plates (Greiner), and a sampling rate of 5

Hz. For most binding and kinetic experiments, ^{sc6}ClpX$^{\Delta N}$-bio (20 nM) was loaded onto

streptavidin biosensors to a BLI response of ~0.5 nm in the absence of nucleotide. In control

experiments, the kinetics of ClpP binding were the same whether ATP was added after or simultaneously with $^{sc6}ClpX^{\Delta N}$-bio loading. For each set of experiments, a control sensor with bound $^{sc6}ClpX^{\Delta N}$-bio, under otherwise identical conditions, was transferred into buffer with no ClpP to determine the baseline and drift. Rates of ATP hydrolysis by $^{sc6}ClpX^{\Delta N}$-bio (200 nM) without or with ClpP (1 μM) were determined at different concentrations of ATP using a coupled assay.[38]

Data analysis. Kinetic trajectories were fit to single- or double-exponential functions using non-linear-least-squares algorithms implemented in Prism (GraphPad Software) or KaleidaGraph (Synergy Software). Trajectories were initially fit to a single-exponential function and were subsequently truncated to ~6 half-lives based on the estimated rate constant. Trajectories longer than 10 s were decimated to 0.5 Hz. The dependence of binding or kinetics on ClpP concentration, ATP concentration, or ADEP-2B concentration was fitted to appropriate equations using Prism or KaleidaGraph.

References

(1) Baker, T.A., and Sauer, R.T. (2012) ClpXP, an ATP-powered unfolding and protein-degradation machine. *Biochim. Biophys. Acta 1823*, 15–28.

(2) Grimaud, R., Kessel, M., Beuron, F., Steven, A.C., and Maurizi, M.R. (1998) Enzymatic and structural similarities between the Escherichia coli ATP-dependent proteases, ClpXP and ClpAP. *J. Biol. Chem. 273*, 12476–12481.

(3) Jones, J.M., Welty, D.J., and Nakai, H. (1988) Versatile action of *Escherichia coli* ClpXP as protease or molecular chaperone for bacteriophage Mu transposition. *J. Biol. Chem. 273*, 459–465.

(4) Burton, R.E., Baker, T.A., and Sauer, R.T. (2003) Energy-dependent degradation: Linkage between ClpXP-catalyzed nucleotide hydrolysis and protein-substrate processing. *Protein Sci. 12*, 893–902.

(5) Joshi, S.A., Hersch, G.L., Baker, T.A., and Sauer, R.T. (2004) Communication between ClpX and ClpP during substrate processing and degradation. *Nat. Struct. Mol. Biol. 11*, 404–411.

(6) Martin, A., Baker, T.A., and Sauer, R.T. (2005) Rebuilt AAA+ motors reveal operating principles for ATP-fueled machines. *Nature 437*, 1115–120.

(7) Stinson, B.M., Nager, A.R., Glynn, S.E., Schmitz, K.R., Baker, T.A., and Sauer, R.T. (2013) Nucleotide binding and conformational switching in the hexameric ring of a AAA+ machine. *Cell 153*, 628–639.

(8) Stinson, B.M., Baytshtok, V., Schmitz, K.R., Baker, T.A., and Sauer, R.T. (2015) Subunit asymmetry and roles of conformational switching in the hexameric AAA+ ring of ClpX. *Nat. Struct. Mol. Biol. 22*, 411–416.

(9) Iosefson, O., Nager, A.R., Baker, T.A. and Sauer, R.T. (2015a) Coordinated gripping of substrate by subunits of a AAA+ proteolytic machine *Nat. Chem. Biol. 11*, 201–206.

(10) Aubin-Tam, M.E., Olivares, A.O., Sauer, R.T., Baker, T.A., and Lang, M.J. (2011) Single-molecule protein unfolding and translocation by an ATP-fueled proteolytic machine. *Cell 145*, 257–267.

(11) Maillard, R.A., Chistol, G., Sen, M., Righini, M., Tan, J., Kaiser, C.M., Hodges, C., Martin, A., and Bustamante, C. (2011) ClpX(P) generates mechanical force to unfold and translocate its protein substrates. *Cell 145*, 459–469.

(12) Sen, M., Maillard, R.A., Nyquist, K., Rodriguez-Aliaga, P., Pressé, S., Martin, A., and Bustamante, C. (2013) The ClpXP protease unfolds substrates using a constant rate of pulling but different gears. *Cell 155*, 636–646.

(13) Cordova, J.C, Olivares, A.O., Shin, Y., Stinson, B.M., Calmat, S., Schmitz, K.R., Aubin-Tam, M-E. Baker, T.A., Lang, M.J., and Sauer R.T. (2014) Stochastic but highly coordinated protein unfolding and translocation by the ClpXP proteolytic machine. *Cell 158*, 647–658.

(14) Olivares, A.O., Nager, A.R., Yosefson, O., Sauer, R.T. and Baker, T.A. (2014) Mechanochemical basis of protein degradation by a double-ring AAA+ machine. *Nat. Struct. Mol. Biol. 21*, 871–875.

(15) Iosefson, O., Olivares, A.O., Baker, T.A. and Sauer, R.T. (2015b) Dissection of axial-pore loop function during unfolding and translocation by a AAA+ proteolytic machine. *Cell Rep. 12*, 1032–1041.

(16) Martin, A., Baker, T.A., and Sauer, R.T. (2007) Distinct static and dynamic interactions control ATPase-peptidase communication in a AAA+ protease. *Mol. Cell 27*, 41–52.

(17) Kim, Y.I., Levchenko, I., Fraczkowska, K., Woodruff, R.V., Sauer, R.T., and Baker, T.A. (2001) Molecular Determinants of Complex Formation between Clp/Hsp100 ATPases and the ClpP Peptidase. *Nat. Struct. Biol. 8*, 230–233.

(18) Singh, S.K., Rozycki, J., Ortega, J., Ishikawa, T., Lo, J., Steven, A.C., and Maurizi, M.R. (2001) Functional domains of the ClpA and ClpX molecular chaperones identified by limited proteolysis and deletion analysis, *J. Biol. Chem. 276*, 29420–29429.

(19) Lee, B.G., Park, E.Y., Lee, K.E., Jeon, H., Sung, K.H., Paulsen, H., Rübsamen-Schaeff, H., Brötz-Oesterhelt, H., Song, H.K. (2010) Structures of ClpP in complex with acyldepsipeptide antibiotics reveal its activation mechanism. *Nat. Struct. Mol. Biol. 17*, 471–478.

(20) Li, D.H., Chung, Y.S., Gloyd, M., Joseph, E., Ghirlando, R., Wright, G.D., Cheng, Y.Q., Maurizi, M.R., Guarné, A., and Ortega, J. (2010) Acyldepsipeptide antibiotics induce the formation of a structured axial channel in ClpP: A model for the ClpX/ClpA-bound state of ClpP. *Chem. Biol. 17*, 959–969.

(21) Schmitz, K.R., Carney, D.W., Sello, J.K., and Sauer, R.T. (2014) The crystal structure of *M. tuberculosis* ClpP1P2 suggests a model for peptidase activation by AAA+ partner binding and substrate delivery. *Proc. Natl. Acad. Sci. USA 111*, E4587–4595.

(22) Brötz-Oesterhelt, H., Beyer, D., Kroll, H.-P., Endermann, R., Ladel, C., Schroeder, W., Schroeder, W., Hinzen, B., Raddatz, S., Paulsen, H., Henninger, K., Bandow, J.E., Sahl, H.G., and Labischinski, H. (2005) Dysregulation of bacterial proteolytic machinery by a new class of antibiotics. *Nat. Med. 11*, 1082–1087.

(23) Kirstein, J., Hoffmann, A., Lilie, H., Schmidt, R., Rübsamen-Waigmann, H., Brötz-Oesterhelt, H., Mogk, A., and Turgay, K. (2009) The antibiotic ADEP reprogrammes ClpP, switching it from a regulated to an uncontrolled protease. *EMBO Mol. Med. 1*, 37–49.

(24) Abdiche, Y., Malashock, D., Pinkerton, A., and Pons, J. (2008) Determining kinetics and affinities of protein interactions using a parallel real-time label-free biosensor, the Octet. *Anal. Biochem. 377*, 209–217.

(25) Shin, Y., Davis, J.H., Brau, R.R., Martin, A., Kenniston, J.A., Baker, T.A., Sauer, R.T., and Lang, M.J. (2009) Single-molecule denaturation and degradation of proteins by the AAA+ ClpXP protease. *Proc. Natl. Acad. Sci. USA 106*, 19340–19345.

(26) Glynn, S.E., Nager, A.R., Baker, T.A., and Sauer, R.T. (2012) Dynamic and static components power unfolding in topologically closed rings of a AAA+ proteolytic machine. *Nat. Struct. Mol. Biol. 19*, 616–622.

(27) Lee, M.E., Baker, T.A., and Sauer, R.T. (2010) Control of substrate gating and translocation into ClpP by channel residues and ClpX binding. *J. Mol. Biol. 399*, 707–718.

(28) Carney, D., Schmitz, K.R., Truong, J., Sauer, R.T., and Sello, J.K. (2014) Restriction of the conformational dynamics of the cyclic acyldepsipeptide macrocycle improves antibacterial

activity by enhancing both ClpP peptidase binding and activation. *J. Amer. Chem. Soc. 136*, 1922–1929.

(29) Glynn, S.E., Martin, A., Nager, A.R., Baker, T.A., and Sauer, R.T. (2009) Crystal structures of asymmetric ClpX hexamers reveal nucleotide-dependent motions in a AAA+ protein-unfolding machine. *Cell 139*, 744–756.

(30 Hersch, G.L., Burton, R.E., Bolon, D.N., Baker, T.A., and Sauer, R.T. (2005) Asymmetric interactions of ATP with the AAA+ $ClpX_6$ unfoldase: allosteric control of a protein machine. *Cell 121*, 1017–1027.

(31) Nager, A.R., Baker, T.A. & Sauer, R.T. (2011) Stepwise unfolding of a β-barrel protein by the AAA+ ClpXP protease. *J. Mol. Biol. 413*, 4-16.

(32) Kenniston, J.A., Baker, T.A., Fernandez, J.M., and Sauer, R.T. (2003) Linkage between ATP consumption and mechanical unfolding during the protein processing reactions of an AAA+ degradation machine. *Cell 114*, 511–520.

(33) Too, P.H., Erales, J., Simen, J.D., Marjanovic, A., and Coffino, P. (2013) Slippery substrates impair function of a bacterial protease ATPase by unbalancing translocation versus exit. *J. Biol. Chem. 288*, 13243–13257.

(34) Vass, R.H., and Chien P. (2013) Critical clamp loader processing by an essential AAA+ protease in *Caulobacter crescentus. Proc. Natl. Acad. Sci. USA 110*, 18138–18143.

(35) Sauer, R.T., and Baker, T.A. (2011) AAA+ proteases: ATP-fueled machines of destruction. *Ann. Rev. Biochem. 80*, 587–612.

(36) Park, S., Li, X., Kim, H.M., Singh, C.R., Tian, G., Hoyt, M.A., Lovell, S., Battaile, K.P., Zolkiewski, M., Coffino, P., Roelofs, J., Cheng, Y., and Finley, D. (2013) Reconfiguration of the proteasome during chaperone-mediated assembly. *Nature 497*, 512–516.

(37) Beckett, D., Kovaleva, E., and Schatz, P.J. (1999) A minimal peptide substrate in biotin holoenzyme synthetase-catalyzed biotinylation. *Protein Sci. 8*, 921–929.

(38) Nørby, J. (1988) Coupled assay of Na+,K+-ATPase activity. *Methods Enz. 156*, 116–119.

Chapter Three:

Roles of the ClpX IGF loops in ClpP association,

dissociation, and protein degradation.

Abstract

The IGF loops of hexameric rings of the AAA+ ClpX unfoldase are required for docking with the self-compartmentalized ClpP peptidase, which consists of two heptameric rings. Here we show that ATP or ATPγS are needed for ClpXP docking because these nucleoside triphosphates change the conformation of the ClpX ring, bringing the IGF loops closer to each other and allowing efficient multivalent contacts with hydrophobic docking clefts on ClpP rings. In single-chain ClpX pseudohexamers, deletion of one or two IGF loops slows association with ClpP modestly but has a major impact in accelerating dissociation of ClpXP complexes. ClpX pseudohexamers with three IGF loops fail to associate stably with ClpP and may be similar to transient encounter intermediates during stepwise assembly of stable ClpXP complexes. We probe how changes in the sequence and length of the IGF loops affect ClpXP interactions and show that deletion of one or two IGF loops slows ClpXP degradation by reducing the rate of polypeptide translocation through the ClpX axial pore and into the proteolytic chamber of ClpP. We also find that ClpXP degradation is less processive when two IGF loops are deleted, resulting in dissociation during translocation of unfolded segments of a multidomain substrate.

Introduction

Within the cells of all organisms, ring hexamers belonging to the AAA+ (ATPases Associated

with various cellular Activities) superfamily of enzymes carry out a wide variety of protein

remodeling, unfolding, and degradation reactions (Hanson & Whiteheart 2005; Baker & Sauer

2012). These ATP-fueled molecular machines typically function by engaging a peptide tag and

pulling the attached native protein against a narrow axial pore, eventually resulting in unfolding

and subsequent translocation through the pore (Kenniston et al. 2003; Martin et al. 2005; Martin

et al. 2007). This activity is essential for the biological function of AAA+ proteases, which

destroy specific intracellular proteins by unfolding them and then translocating the denatured

polypeptide into the chamber of a self-compartmentalized peptidase for degradation (Baker &

Sauer 2012).

For example, the ClpX unfoldase and ClpP peptidase comprise the AAA+ ClpXP protease,

which degrades a variety of cellular proteins in addition to proteins modified by co-translational

addition of the ssrA tag in *Escherichia coli* and many other bacteria (Keiler et al. 1996; Farrell et

al. 2005). ClpP consists of two heptameric rings, stacked face-to-face, that enclose a proteolytic

chamber. Each heptameric ClpP ring can bind one ClpX hexamer, giving rise to symmetry

mismatched singly-capped (XP) or doubly-capped (XPX) complexes (Ortega et al. 2002; Singh

et al. 2001). These ClpXP complexes are largely stabilized by peripheral interactions in which

IGF loops from ClpX dock into hydrophobic clefts on the surface of a ClpP ring (Fig. 3.1A, Fig.

3.1B) (Martin et al. 2007; Ortega et al. 2002; Singh et al. 2001; Amor et al. 2016; Joshi et al.

2004). The IGF loops are named for a tripeptide in the loop sequence that is very highly

conserved in ClpX orthologs from proteobacteria (Fig. 3.1C, top panel) but can be MGF, LGF,

etc. in other bacterial phyla (Fig. 3.1C, bottom panel). The AAA+ ClpA unfoldase contains

related loops with an IGF-like tripeptide and also collaborates with ClpP in protein degradation (Kim et al. 2001; Kim et al. 2000). The hydrophobic clefts on ClpP also bind acyldepsipeptides (ADEPs), which compete for ClpX or ClpA binding to ClpP (Lee et al. 2010a; Schmitz et al. 2014; Amor et al. 2016). ADEPs can kill bacteria by opening the narrow ClpP portal, allowing rogue degradation of nascent proteins and other unfolded or poorly structured proteins (Conlon et al. 2013). Previous studies of *E. coli* ClpX show that mutating the IGF tripeptide to <u>E</u>GF or IG<u>W</u> severely compromises ClpP binding and function (Kim et al. 2001). Deleting one or two IGF loops from single-chain pseudohexamers consisting of genetically linked ClpX subunits also results in ClpP-binding defects (Martin et al. 2007). ClpX binding to ClpP requires ATP or ATPγS, an analog that ClpX hydrolyzes slowly, but the basis for this nucleoside-triphosphate requirement is unknown (Hersch et al. 2005; Amor et al. 2016). Here, we investigate the molecular mechanism that underlies the ATP-dependence of ClpX binding to ClpP and determine how changes in the number, geometric distribution, sequence, and length of IGF loops in hexamers of *E. coli* ClpX impact its binding to ClpP and its ability to carry out ATP-dependent protein degradation.
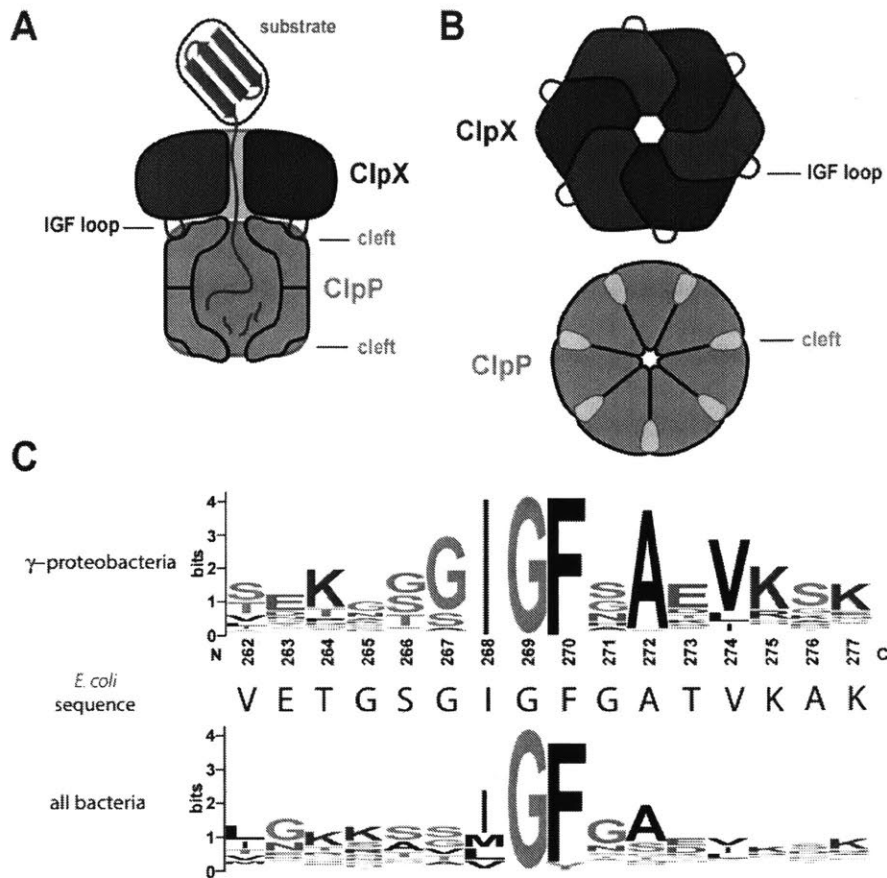
Figure 3.1. A. Cartoon of the ClpXP protease degrading a protein substrate. The ClpX hexamer (colored purple and blue) recognizes a protein substrate (colored green) and uses cycles of ATP hydrolysis to unfold and translocate it into the degradation chamber of the ClpP peptidase (colored dark yellow). The IGF loops of ClpX dock into hydrophobic clefts on ClpP. **B.** Top views of the ClpX and ClpP rings, highlighting the six IGF loops of ClpX and seven clefts of ClpP. **C.** Sequence-logo depictions of sequence conservation in the IGF loops of ClpX orthologs from γ-proteobacteria (top) and all bacteria (bottom) (Crooks et al. 2004). The sequence of the *E. coli* ClpX IGF loop is shown in the middle.

Results

Nucleotide effects on accessibility of ClpX IGF-loops. Prior experiments show that the IGF loops in the ClpX hexamer can be rapidly cleaved by proteases (Singh et al. 2001). We used proteolytic cleavage to test if different nucleotides changed the accessibility of the IGF loops in

ClpX$^{\Delta N}$, a variant lacking the N-domain that is still fully active in binding ClpP and supporting

degradation of ssrA-tagged substrates (Martin et al. 2005; Stinson et al. 2013; Glynn et al. 2009;

Martin et al. 2008). As shown in the top gel of Fig. 3.2A, chymotrypsin cleaved ClpX$^{\Delta N}$ at one

major site to generate fragments of ~24 and ~17 kDa. These fragments were not produced when

ClpX$^{\Delta N}$ variants harbored a deletion of the IGF loop or the F270A mutation in the IGF loop,

establishing that chymotrypsin cleaves ClpX$^{\Delta N}$ within the IGF-loop, probably immediately after

Phe^{270}. As ClpX$^{\Delta N}$ starts at residue 63, cleavage after Phe^{270} would generate an N-terminal

fragment of 23.6 kDa and C-terminal fragment of 17.4 kDa. Importantly, the ClpX$^{\Delta N}$

chymotryptic fragmentation pattern and cleavage kinetics were very similar in experiments

performed in the presence of ATP, ATPγS, or ADP (Fig. 3.2B). This finding suggests that the

IGF tripeptides in the hexamer are roughly equally accessible irrespective of the identity of

bound nucleotide. Hence, the failure of ADP-bound ClpX to bind ClpP is not a consequence of

the IGF-loops being sequestered or assuming a protease-resistant structure in the presence of
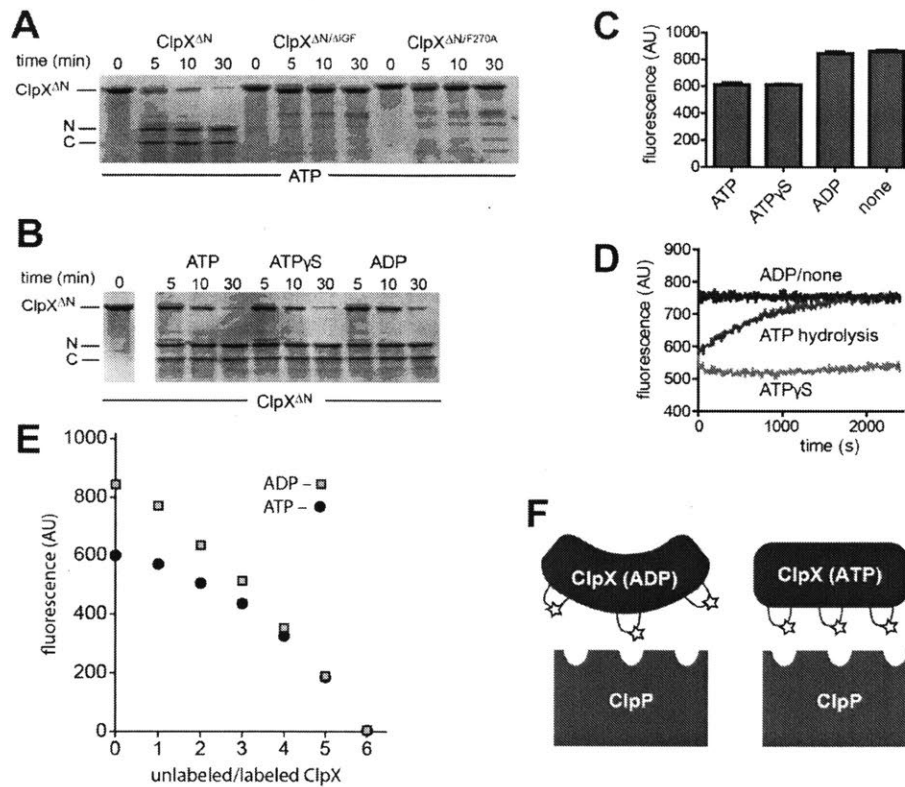
ADP.

Figure 3.2. Nucleotide dependence of protease accessibility and relative distance between IGF loops. **A.** As assayed by SDS-PAGE, chymotrypsin cleaved ClpX$^{\Delta N}$ into two major fragments, labeled N and C, which were not observed following chymotrypsin incubation with ClpX$^{\Delta N/\Delta IGF}$ or ClpX$^{\Delta N/F270A}$. Experiments contained ATP (10 mM), chymotrypsin (0.01 mg/mL), and ClpX$^{\Delta N}$ variants (1 μM hexamer). **B.** Chymotryptic cleavage of ClpX$^{\Delta N}$ in the presence of different nucleotides. With the exception of nucleotide identity, experimental conditions were the same as in panel A. **C.** Initial fluorescence of Alexa-647 labeled ClpX$^{\Delta N/T273C}$ (excitation 620 nm; emission 671 nm) after addition of ATP, ATPγS, ADP, or without nucleotide addition. The protein concentration was 0.5 μM, and nucleotide was 1.5 mM when present. Values are averages (N=3) ± SD. **D.** Time dependent changes in fluorescence of Alexa-647 labeled ClpX$^{\Delta N/T273C}$ under different nucleotide conditions. Other conditions were identical to panel C. **E.** Unlabeled ClpX$^{\Delta N/T273C}$ was mixed with different amounts of Alexa-647 labeled ClpX$^{\Delta N/T273C}$ for 1 h in the absence of nucleotide, 5 mM ADP or ATPγS was then added, and the fluorescence was measured. **F.** Increased homo quenching and decreased fluorescence is consistent with the IGF loops being closer together in fluorescent ClpX$^{\Delta N/T273C}$ that is bound to ATP compared to ADP. We proposed that the IGF loops in ATP-bound ClpX are properly oriented to make efficient multivalent contacts with the clefts in ClpP, whereas the IGF-loops in ADP-bound ClpX can only make a subset of efficient contacts.

Nucleotides affect IGF-loop proximity. The experiments in this section were performed using a variant of $ClpX^{\Delta N}$ bearing the T273C mutation, which introduces an exposed cysteine in the IGF-loop to allow labeling with a fluorescent dye. $^{T273C}ClpX^{\Delta N}$ supported robust ClpP degradation of GFP-ssrA (not shown). We labeled $^{T273C}ClpX^{\Delta N}$ with Alexa-647-C2-maleimide. The excitation and emission spectra of the Alexa-647 fluorophore overlap substantially, allowing homo quenching if two or more labeled IGF loops are sufficiently close to each other in the hexamer. The fluorescence of labeled $^{T273C}ClpX^{\Delta N}$ was similar in the absence of nucleotide or presence of 1 mM ADP, but decreased ~30% in the presence of 1 mM ATP or ATPγS (Fig. 3.2C). Fluorescence remained constant as a function of time for the no-nucleotide or ADP experiments and increased very slowly for the ATPγS sample (Fig. 3.2D). For the ATP sample, by contrast, fluorescence increased over the course of ~30 min to the level of the ADP sample (Fig. 3.2D), presumably because most of the ATP initially present was hydrolyzed over this time period.

Two models could explain why ATP/ATPγS-bound ClpX hexamers have lower fluorescence than ADP-bound or nucleotide-free hexamers. First, the IGF-loops could be closer to each other in ATP/ATPγS-bound hexamers and farther apart in ADP-bound or nucleotide-free hexamers. Second, decreased fluorescence in the presence of ATP/ATPγS might result from local changes in the environment of individual IGF-loops rather than changes in global proximity of different IGF-loops. To distinguish between these models, we mixed different ratios of unlabeled protein and fluorescently labeled protein for 1 h in the absence of nucleotide to allow subunit exchange, and then added ATPγS or ADP before assaying fluorescence. The local-environment model predicts a linear decrease in fluorescence as a function of the ratio of labeled to unlabeled protein, but significant non-linear changes were observed for ADP and strong non-linear changes

were seen in the ATPγS experiment (Fig. 3.2E). We conclude that the IGF-loops in a ClpX

hexamer are closer together in ATP-bound or ATPγS-bound enzymes and farther apart in ADP-

bound or nucleotide-free enzymes, implying a substantial ATP-dependent conformational change

in the ClpX hexamer that positions the IGF-loops for efficient multivalent docking with ClpP

(Fig. 3.2F).

Effects of IGF-loop removal on ClpX association with ClpP. Bio-layer interferometry (BLI)

allows the kinetics of ClpX binding to ClpP to be followed in real time (Amor et al. 2016). We

used single-chain ClpX$^{\Delta N}$ pseudohexamers with a single biotinylation site near the C-terminus,

attached this protein to a streptavidin-coated biosensor, and assayed ClpP association via

changes in the BLI-response signal. We constructed and purified variants in which we replaced

one or two IGF loops with GGSSGG linkers. In the single-chain hexamer, subunit A is at the N-

terminus, subunits B, C, D, and E follow in order, and subunit F is at the C-terminus. The single

IGF deletion/substitution was in subunit B, and the double deletion/substitutions were in subunits

AB, BC, BD, or BE. For each variant, we fit the association trajectories in the presence of ATP

to a double exponential (the variant with six IGF loops showed a major fast phase and minor

slow phase) or single exponential (all variants with four or five IGF loops) to determine apparent

association rate constants (k_{app}) at different concentrations of ClpP. We then determined the

association-rate constant (k_{assn}) from either a linear fit (see, for example, Fig. 3.3A) or hyperbolic

fit (see, for example, Fig. 3.3B) of these data. For the parental enzyme with six IGF loops, k_{assn}

for the major phase was ~$1.3 \cdot 10^6$ M^{-1}s^{-1}. This value was reduced to ~$2 \cdot 10^5$ M^{-1}s^{-1} for the variant

with four or five IGF loops, irrespective of the configuration (Fig. 3.3C). Thus, removal of one

or two IGF loops slows binding ~6-fold, a value greater than would be expected from the simple

fraction of IGF loops remaining in the hexamer. This finding suggests that binding is a multistep

process with formation of metastable complexes preceding formation of a stable complex (see Discussion). We also tested a ClpX$^{\Delta N}$ variant in which three IGF loops (in subunits A, B, and C) were deleted, but in our BLI experiments, no significant ClpP binding was detected to this mutant enzyme.
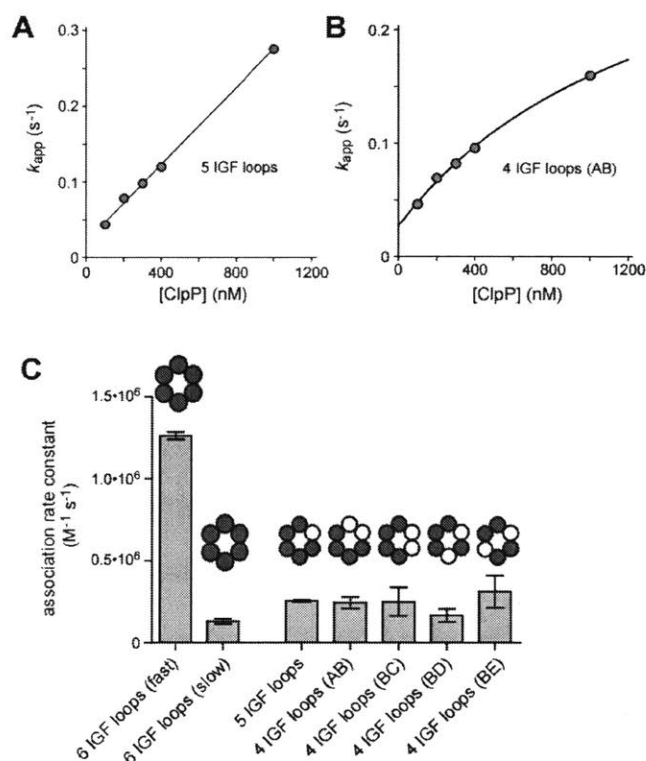

Figure 3.3. Effects of deletion of IGF loops on the rate of ClpP association with ClpX. **A.** Effects of ClpP concentration on the apparent association rate constant (k_{app}) to single-chain ClpX$^{\Delta N}$ with five IGF loops immobilized on a BLI sensor. The slope of the linear fit is the second-order association rate constant (k_{assn}). **B.** For single-chain ClpX$^{\Delta N}$ with four IGF loops (loops in subunits AB deleted), k_{app} varied hyperbolically with ClpP concentration. The line is a non-linear-least-squares fit to the equation $k_{app} = \text{max} \cdot [ClpP]/(K_{1/2}+[ClpP])$, and $k_{assn} = \text{max}/K_{1/2}$. Other variants with four IGF loops also displayed hyperbolic variation of k_{app} with ClpP concentration. **C.** Second-order rate constants for ClpP association to single-chain ClpX$^{\Delta N}$ variants with different numbers and configurations of IGF-loop deletions determined from experiment like those shown in panels A and B. Values are averages (N=3) ± SD. All association experiments in this panel contained 2 mM ATP.

Dissociation kinetics and degradation. To assay dissociation kinetics, we allowed ClpXP complexes to assemble in the presence of ATP, and then shifted the BLI biosensor into buffer containing ATP but no ClpP (Fig. 3.4A). As seen previously (Amor et al. 2016), wild-type complexes were very stable, with no detectable dissociation observed over the course of several hours. Deletion of one IGF loop resulted in dissociation with a half-life of ~500 s (Fig. 3.4A), but the amplitude of the single-exponential fit was ~50% of the expected value, suggesting that there are two populations of complexes, one longer lived and one shorter lived. We obtained the same result in experiments using a different preparation of this variant, suggesting that biphasic dissociation was not a result of enzyme heterogeneity. Moreover, experiments in which we dipped the biosensor into fresh ClpP-free buffer several times gave the same result, establishing that failure to dissociate completely over the course of several hours is not a consequence of reaching equilibrium. Deletion of two IGF loops reduced the half-life of the complex to ~30-40 s, irrespective of the configuration of the subunits containing the deletions (Figs. 3.4A, 3.4B). Thus, the ClpXP complex becomes dramatically less stable as an increasing number of IGF-loops are removed from the hexamer.
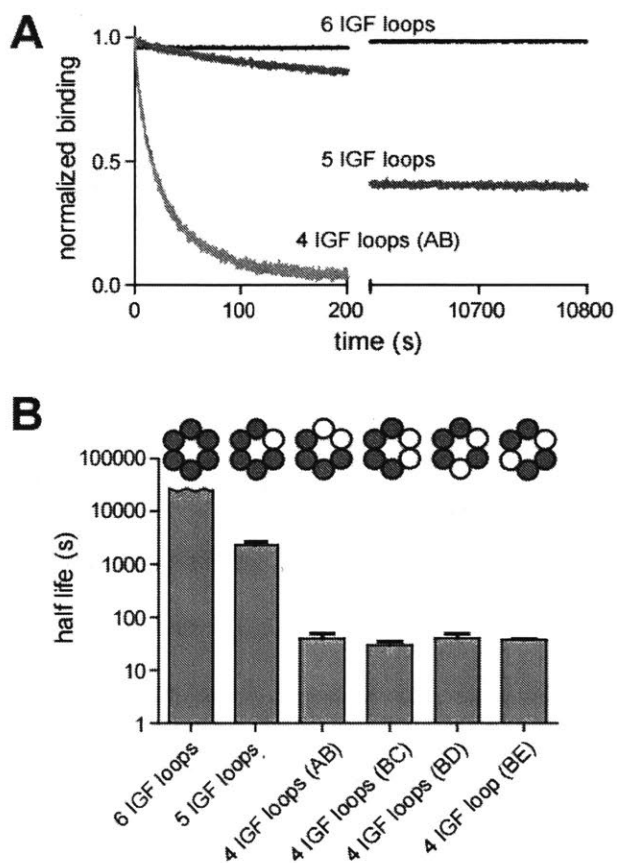
Figure 3.4. Effect of IGF-loop deletion on dissociation kinetics. **A.** Dissociation kinetics for complexes of ClpP and different variants of single-chain ClpX$^{\Delta N}$ were measured in 1 mM ATP by monitoring changes in BLI response following transfer of the biosensor into buffer lacking ClpP. **B.** Half-lives were calculated from single exponential fits of dissociation experiments like those shown in panel A. The half-life for the variant with six IGF loops is a lower limit. Values are averages (N=3) ± SD.

We also tested the ability of the variants missing one or two IGF loops to support ClpP degradation of GFP-ssrA (Fig. 3.5A). Compared to the parental ClpX$^{\Delta N}$ pseudohexamer, deletion

of one loop decreased the degradation rate ~2-fold, whereas deletion of two loops decreased the degradation rate ~5-fold. The reduced activity of the deletion mutants is unlikely to result from an inability to form ClpXP complexes, as affinities predicted from the association and dissociation kinetics were 120 nM or tighter, whereas the ClpP concentration in the degradation experiments was 900 nM. It is also unlikely that reduced degradation is a consequence of a reduced rate of substrate unfolding, as the variants with four, five, or six IGF loops unfolded an Arc-GCN4 dimer at similar rates in the absence of ClpP (Fig. 3.5B). We propose that docking of all six IGF-loops in the hexamer is required to fully open the axial channel into ClpP. This model predicts that the docking of the deletion mutants with ClpP results in a narrower axial channel, either statically or because the channel equilibrates between open and closed states, making translocation into ClpP more difficult.
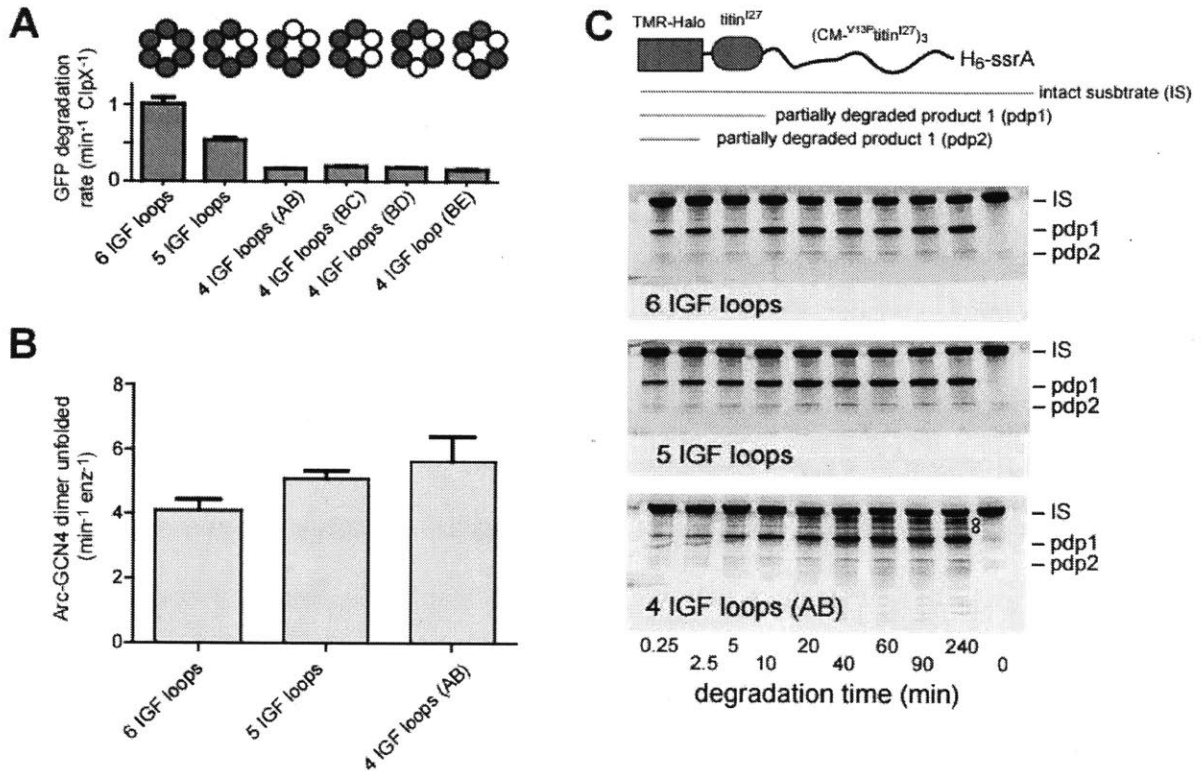
Figure 3.5. IGF-loop deletion affects degradation rates and processivity. **A.** Rates of degradation of GFP-ssrA (20 µM) by ClpP (0.9 µM) and different variants of ClpX (0.3 µM pseudohexamer) were measured by monitoring loss of GFP fluorescence. Values are averages (N=3) ± SD. **B.** Rates of unfolding of a fluorescent Arc-GCN4 dimer (5 µM) by ClpX variants (0.3 µM pseudohexamer) were measured as described in the presence of 10 mM ATP (Baytshtok, Baker, and Sauer 2015). **C.** Top; diagram of a multidomain substrate containing a TAMRA-labeled Halo domain, a native titin[I27] domain, three [V13P]titin[I27] domains unfolded by carboxymethylation (CM), and a H_6-ssrA degron. Bottom; SDS-PAGE assays of the ClpP degradation of this substrate by ClpX[ΔN] variants with six, five, or four IGF loops. Note that the variant with four IGF loops shows multiple additional bands between IS and pdp1, indicative of poorly processive degradation. Reactions contained substrate (10 µM), 0.9 µM ClpP, 0.3 µM single-chain ClpX[ΔN] variants (hexamer equivalents), and 10 mM ATP. Gels were imaged for fluorescence of the TAMRA dye.

We also tested degradation of a multidomain substrate consisting of an N-terminal Halo domain labeled with a TAMRA dye, a native $titin^{I27}$ domain, three $^{V13P}titin^{I27}$ domains unfolded by carboxymethylation of normally buried cysteines, an H_6 sequence, and a C-terminal ssrA tag (Fig. 3.5C, top) (Iosefson et al. 2015). Previous studies show that $ClpX^{\Delta N}$ and ClpP efficiently degrade the unfolded domains of this substrate but a partially degraded product (pdp1) consisting of the Halo and native $titin^{I27}$ domains accumulates as a consequence of some enzymes dissociating after failing to unfold $titin^{I27}$ (Iosefson et al. 2015; Kenniston et al. 2005). As assayed by SDS-PAGE and fluorescence imaging, the pdp1 product was observed during ClpP degradation supported by single-chain $ClpX^{\Delta N}$ variants with six, five, or four IGF loops, but this product accumulated more slowly as more IGF loops were removed (Fig. 3.5C). For example, the pdp1 product accumulated at 57% of the wild-type rate for the single IGF deletion and at 34% of this rate for the double IGF deletion, supporting the idea that translocation in ClpP may slow as more IGF loops are deleted. Notably, fragments intermediate in size between the intact substrate (IS) and pdp1 product were observed for the $ClpX^{\Delta N}$ variant containing four IGF loops (marked by circles in lower gel of Fig. 3.5C) but not for enzymes containing five or six IGF loops. This result indicates that degradation by the variant with four IGF loops is less processive and that some enzymes dissociate during translocation of unfolded portions of the substrate.

Replacing the ClpX IGF-loop with the ClpA IGL-loop . Hexamers of *E. coli* ClpA can also collaborate with ClpP in protein degradation. Thus, we asked if the IGF-loop of ClpX could be replaced with the related IGL-loop from ClpA. We found, however, that a $ClpX^{\Delta N}$ variant bearing the loops of ClpA ($ClpX^{\Delta N/swap}$) showed major defects in ClpP degradation of GFP-ssrA (Fig. 3.6A). Moreover, ClpP binding normally suppresses the rate at which ClpX hydrolyzes ATP ~2-fold, whereas the ATPase activity of the loop-swap mutant did not change when ClpP

was present (Fig. 3.6B). The ClpX and ClpA loops have very different amino-acid sequences. For example, to generate ClpX$^{\Delta N/swap}$ the IGF-loop sequence ETGSG<u>IGF</u>GATVK from ClpX was replaced with TERKS<u>IGL</u>IHQDN from ClpA, maintaining loop length but changing the identities of 11/13 residues.
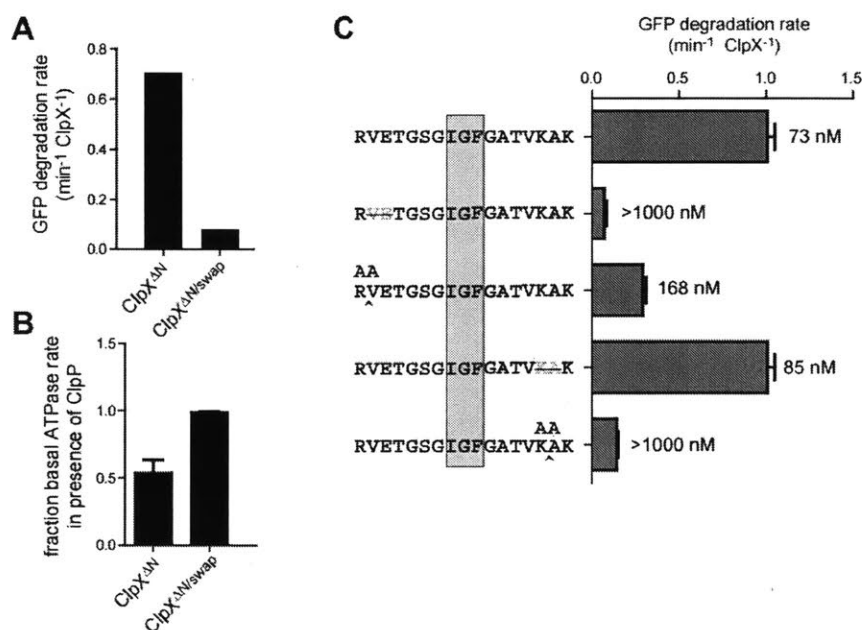

Figure 3.6. IGF-loop swap and length mutations. **A.** Degradation of GFP-ssrA (20 µM) by ClpP (0.9 µM) and either ClpX$^{\Delta N}$ (0.3 µM hexamer) or a variant containing the IGL loop from *E. coli* ClpA (ClpX$^{\Delta N/swap}$; 0.3 µM hexamer). **B.** Suppression of the rate of hydrolysis of ATP (10 mM) by ClpX$^{\Delta N}$ or ClpX$^{\Delta N/swap}$ (0.3 µM hexamer) by addition of ClpP (0.9 µM). **C.** Rates of degradation of GFP-ssrA (20 µM) by ClpP (0.9 µM) and ClpX$^{\Delta N}$ variants containing longer or shorter IGF loops (0.3 µM hexamer). Numbers next to the degradation bars represent the affinity of each mutant for ClpP determined by a pore-opening assay (M. E. Lee, Baker, and Sauer 2010b). In all panels, values are averages (N=3) ± SD.

Loop-length mutations. In an unlinked ClpX$^{\Delta N}$ background, we found that deletion of two residues from the C-terminal part of the IGF-loop did not substantially impact the rate of ClpP degradation of GFP-ssrA or the affinity of ClpP binding as assayed by peptidase activation (Fig.

3.6C). However, major degradation defects and weakened ClpP affinity was observed after deletion of two residues from the N-terminal part of the loop (Fig. 3.6C). Insertion of two additional alanines in either the N-terminal or C-terminal parts of the IGF loop also caused slower degradation and/or weakened affinity. Thus, some changes in IGF-loop length are tolerated, whereas others are not. The ClpX IGF loop is 16 residues in length. When we calculated IGF-loop lengths for a large number of ClpX orthologs, the most common lengths were 14 or 15 residues with a range from 8-16 residues.

Substitution mutations in the IGF loop. Mutation of Ile^{268} to Ala, Val, or Leu, changing Phe^{270} to Ala, Val, Ile, or Leu, and replacing Val^{274} with Ala severely compromised or eliminated the ability of unlinked $ClpX^{\Delta N}$ to collaborate with ClpP in degrading GFP-ssrA (Fig. 3.7A). Moreover, ClpP did not suppress the rate of ATP hydrolysis by these variants (Fig. 3.7B). Other amino-acid substitutions at non-alanine and non-glycine positions in the IGF loop of $ClpX^{\Delta N}$ – including V262A, E263A, T264A, S266A, T273A, K275A, and K277A – had little effect on degradation or ClpP-dependent changes in ATP hydrolysis (Figs. 3.7A, 3.7B).
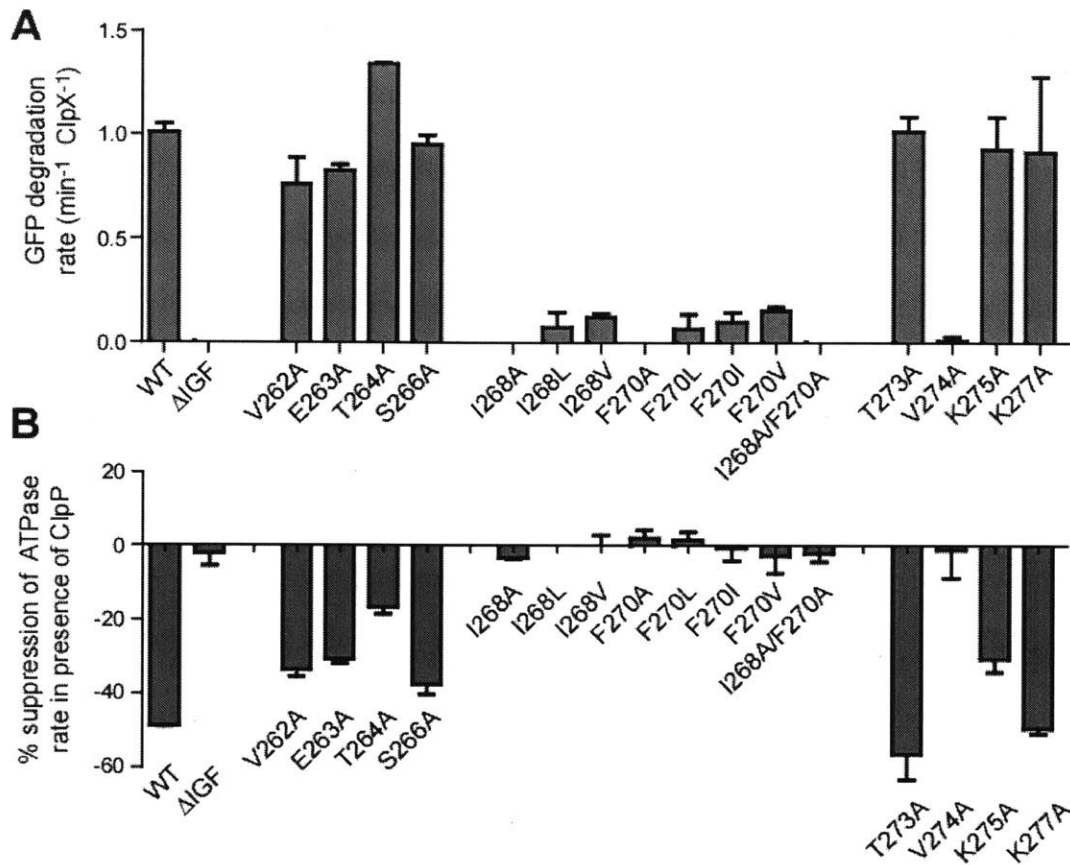
Figure 3.7. Mutations in the IGF loop. **A.** Rates of degradation of GFP-ssrA (20 μM) by ClpP (0.9 μM) and ClpX$^{\Delta N}$ variants (0.3 μM hexamer) with single or double residue substitutions in the IGF loop. **B.** Suppression of the rate of hydrolysis of ATP (10 mM) by IGF loop variants (0.3 μM hexamer) upon addition of ClpP (0.9 μM). In all panels, values are averages (N=3) ± SD.

The experiments described above identify the side chains of Ile^{268}, Phe^{270}, and Val^{274} in the IGF loop as being very important for ClpP binding and/or functional collaboration. To further probe the relative importance of these three positions, we also constructed single-chain ClpX$^{\Delta N}$ pseudo hexamers containing an IGF-loop deletion in subunit B and I268A, F270A, I268A/F270A, or V274A mutations in subunit A. Because deletion of a single IGF-loop slows dissociation to a measurable rate, we reasoned that effects of the mutations in subunit A on association and dissociation kinetics could be detected in BLI experiments. The single and double point

mutations had small effects on the rate of association (Fig. 3.8A) but more substantial effects on

the rate of dissociation (Fig. 3.8B). Specifically, faster dissociation followed the trend ΔIGF >

I268A/F270A > F270A > I268A > V274A.
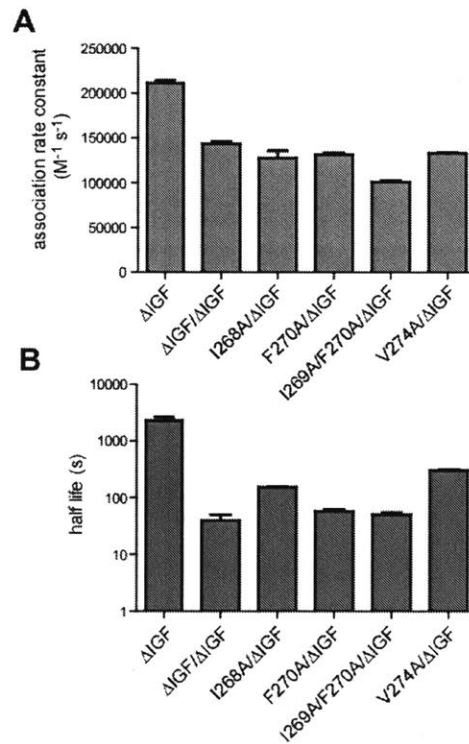
Figure 3.8. Effects of mutations in the IGF motif on ClpP association and dissociation. Single-chain ClpX$^{\Delta N}$ variants had the IGF-loop deleted from subunit B and had a wild-type or mutant IGF motif in subunit A. **A.** Association rate constants determined by BLI experiments using 1 µM ClpP and 2 mM ATP. **B.** Dissociation half lives determined by BLI experiments in the presence of 2 mM ATP.

Discussion

The IGF loops of ClpX are disordered in most crystal structures, suggesting that they are

statically or dynamically disordered (Glynn et al. 2009; Stinson et al. 2013). Indeed, flexibility of

these loops was initially postulated as a mechanism to overcome the symmetry mismatch

between the hexameric ring of ClpX and heptameric rings of ClpP (Kim & Kim 2003). If these loops are flexible, however, then why is ATP or ATPγS is needed to support ClpXP assembly? Our results indicate that the IGF loops are equally accessible to chymotryptic cleavage in the presence of ATP, ATPγS, or ADP. Thus, the inability of ADP to support assembly is not a consequence of the IGF loops being hidden or sequestered. Rather, fluorescence homo-quenching studies indicate that the IGF loops are farther apart in the presence of ADP or absence of nucleotide and closer together in the presence of ATP or ATPγS. Thus, it seems likely ATP and ATPγS alter the conformation of the hexameric ring of ClpX, which places the IGF loops in positions that allow efficient multivalent binding to the clefts on the ClpP ring. We found that a minimum of four IGF loops was required for ClpX to bind ClpP. It is possible, therefore, that ADP-bound or nucleotide-free ClpX can only make three good IGF-loop contacts with ClpP, but that these contacts are not sufficient to form a stable complex.

The precise affinity of single-chain ClpX$^{\Delta N}$ for ClpP is not known because the complex is too kinetically stable to determine an accurate dissociation rate constant. Nevertheless, this K_D appears to be ~100 pM or less (Amor et al. 2016). Based on our studies here, removal of one IGF loop reduces this affinity to ~5 nM, whereas removal of two IGF loops reduces it to ~100 nM. We were unable to detect binding of a ClpX$^{\Delta N}$ variant with three IGF loops to ClpP, but it is not unreasonable to expect that this would occur in the low to medium µM range.

In previous studies at high concentrations of ClpP, we found that the rate of ClpX association saturates hyperbolically (Amor et al. 2016), suggesting that ClpP initially forms an unstable encounter complex with ClpX, which then becomes stabilized by unimolecular docking of more IGF loops. Based on those studies, the major encounter complex formed with a saturated rate of

27 ± 7 s^{-1} (k_2), a half maximal ClpP concentration of ~35 $\pm$ 14 μM ((k_2+k_{-1})/k_1), and an apparent

second-order rate constant ($k_2 \cdot k_1/(k_2+k_{-1})$)) of ~600,000 $\pm$ 80,000 M^{-1}s^{-1}. We solved for values of

k_1 and k_{-1} that would minimize differences with the observed values for the half-maximal

concentration and apparent second-order rate constant. A k_1 value of 10^7 M^{-1}s^{-1} and k_{-1} value of

370 s^{-1} predict half-maximal formation of the encounter complex at ~40 μM ClpP and an

apparent second-order rate constant of ~6.8$\cdot$10^5 M^{-1}s^{-1}, within the error limits of the experimental

values. By this model, the encounter complex would form ~8-fold faster than the stable ClpXP

complex but dissociate at a rate ~14-fold faster than the rate of conversion of the encounter

complex to the stable ClpXP complex. These values seem plausible if the encounter complex

involves docking of two or three ClpX IGF loops with ClpP. Dividing k_2 (the rate of

unimolecular docking of IGF loops) by the second-order association rate constants for ClpX$^{\Delta N}$

variants with six, five, or four IGF loops (bimolecular docking of IGF loops) gives effective

concentrations from approximately 20 to 200 μM. These values seem reasonable for

intramolecular docking of flexible loops in an encounter complex. The trend we observe of faster

dissociation rates as additional IGF loops are deleted is also consistent with a model in which a

transient complex with two or three docked IGF loops could dissociate on the millisecond

timescale. It is possible that ADP-bound ClpX can also form a similar encounter complex but is

then unable to then make additional IGF-loop contacts because of conformational constraints.

Our mutagenic and biochemical studies reveal that substitutions in the first and third residues of

the IGF motif (Ile^{268} and Phe^{270}) can be as deleterious to binding as deletion of the entire loop. In

addition, they show that Val^{274} also plays an important role in stabilizing the ClpXP complex.

Some changes in the length of the IGF loop are tolerated but others were not, suggesting that the

geometry with which the IGF motif and supporting residues are displayed is also an important

determinant of ClpXP binding affinity. We assume that similar factors explain the inability of the IGL loops of ClpA to substitute well for the IGF loops of ClpX in loop-swap studies.

We found that ClpX variants with only four or five IGF loops support rates of ClpP protein degradation that are 20-50% of the rate for the parental enzyme with six IGF loops. Our experiments also suggest that these defects arise not as a consequence of a failure to bind ClpP or of slower protein unfolding but rather because the protein substrate is translocated more slowly into the ClpP chamber. The ClpP axial channel, which gates access into the degradation chamber, is widened upon binding of ClpX or small-molecule ADEPs, which mimic the IGF loops of ClpX (Amor et al. 2016; Schmitz et al. 2014; Lee et al. 2010a). As some ClpX or ADEP binding energy must be used to stabilize the open-channel conformation of ClpP, variants with fewer IGF loops may not be able to fully open the channel or it could equilibrate between open and restricted conformations in these enzymes. Either model could explain slower substrate translocation and thus slower degradation. Notably, we found that a ClpX variant with four IGF loops supported less processive ClpP degradation of a substrate consisting predominantly of unfolded polypeptide segments compared to variants with five or six IGF loops. This result indicates that ClpP dissociates from the four-loop variant in the midst of polypeptide translocation. By contrast, ClpX with a wild-type complement of IGF loops rarely dissociates from ClpP during translocation but can dissociate during failed unfolding of a native substrate domain (Kenniston, 2005).

Methods

Proteins.

ClpP and single-chain $ClpX^{\Delta N}$ pseudohexamers were expressed and purified as described (Amor et al. 2016). Unlinked $ClpX^{\Delta N}$ containing an N-terminal His_6-TEV tag (MGSSHHHHHHDYDIPTTENLYFQGSS) was expressed from pET-22b (EMD Millipore) and purified as described for single-chain $ClpX^{\Delta N}$ (Amor et al. 2016). IGF loop deletions replaced ClpX residues 262-277 with a GGSSGG linker (Hersch et al., 2004). Other mutations were generated by replacing relevant codons with corresponding alanine codons. His_6-TEV-GFP-ssrA was expressed from pET-22b (EMD Millipore) and purified as described (Amor et al. 2016).

Biochemical assays.

Unless noted, biochemical assays were performed at 25 °C in PD buffer (25 mM HEPES, pH 7.5, 100 mM KCl, 10 mM $MgCl_2$, and 10% glycerol) supplemented with ATP, ATPγS, or ADP as necessary. Enzyme concentrations refer to ClpX hexamers and ClpP 14-mers. ATPase activity of $ClpX^{\Delta N}$ was measured by a coupled assay (Nørby 1988). Percent change in ATPase due to ClpP being present was measured at 300 nM $ClpX^{\Delta N}$ and +/- 900 nM ClpP and 5 mM ATP (Sigma). All measurements were taken in clear NBS 384-well plates (Corning) on a SpectraMax M5 plate reader. GFP degradation was measured at 20 μM GFP-ssrA, 300 nM $ClpX^{\Delta N}$, 900 nM ClpP 5 mM ATP, 32 mM phosphocreatine, and 0.064 mg/mL creatine kinase. Rates were measured on a SpectraMax M5 in black NBS 384-well plates (Corning) in triplicate. Degradation was measured as a loss in fluorescence (467 nm excitation, 511 nm emission). Initial rates were calculated from linear fits of the initial loss of fluorescence.

To detect ClpXP binding biochemically, a pore opening assay was used as previously described (Lee et al. 2010b). Dilutions of ClpX$^{\Delta N}$ were mixed with 50 nM ClpP, 15 μM Abz-KASPVSLGY^{NO2}D decapeptide, 2 mM ATP, 32 mg/mL phosphocreatine, and 0.032 mg/mL creatine kinase in PD buffer. Fluorescence of the unquenched dye was measured by excitation at 384 nm and 420 nm emission. Final endpoint fluorescence signal was measured by adding 0.05 mg/mL elastase for 10 min. Linear fits of fluorescence over time and final signals were used to determine rate of peptide cleavage.

To determine protein unfoldase rates were measured using a previously described assay (Baytshtok et al. 2015). Arc^{RC23} repressor harboring a C terminal coil-coil GCNp1 domain, followed by a st11 tag and further followed by a ssrA degron was purified and labeled with Alexa-488-C5 maleimide or Alexa-647-C2-maleimide as previously described (Baytshtok et al. 2015). All assays were performed with 5 μM of Alexa-488 Arc was mixed with equimolar amounts of Alexa-647 Arc after mixing for 1 hr. Then, 0.3 μM ClpX, 32 mM Phosphocreatine, 0.064 mg/mL creatine kinase and 10 mM ATP was added. Unfolding of Arc dimers was measures as a loss of FRET signal at Ex/Em 494/668 nm (Baytshtok et al. 2015) at 25 °C using a SpectraMax M5 plate reader in black 384-well plates (Corning). Final rates were calculated for linear fits of the data with spontaneous background unfolding subtracted

Loop dynamics via Alexa-647 labeling.

10 μM monomerically-encoded ClpX$^{\Delta N}$ T273C was labeled with 90 μM Alexa Fluor 647-C$_2$-Maleimide (ThermoFischer). Protein concentration and labeling efficiency was calculated to be ~6 dyes/hexamer using spectrophotometric measurements and the manufacturer's dye correction factors. Fluorescence measurements (655 nm excitation, 671 nm emission) used 500 nM ClpX$^{\Delta N}$

and 1 mM of the indicated nucleotide when indicated in PD buffer at 25°C. Ratio measurements were made by mixing Alexa-647-labeled T273C ClpX$^{\Delta N}$ with wild type ClpX$^{\Delta N}$ and allowed equilibration for 1 hr prior to addition of nucleotide.

Chymotrypsin digest of ClpX

ClpX$^{\Delta N}$ was digested with chymotrypsin to test for IGF loop exposure. All reactions were done at 1 µM ClpX$^{\Delta N}$ hexamer equivalents, 10 mM nucleotide when indicated, and 0.01 mg/mL chymotrypsin (Worthington) in PD buffer at 25°C. Reactions were initiated with the addition of chymotrypsin. Aliquots were taken at the indicated time points and 1 mM PMSF (Sigma) was added to quench digestion. 10 µL of quenched reaction was then mixed with 2X Sample Buffer (BioRad) and 15 µL was run on a 2-20% gradient SDS-PAGE (GenScript) in 1X MOPS buffer (GenScript). Gels were run for 50 minutes and then stained using Sypro Ruby Gel Stain (BioRad) according to the provided rapid staining protocol. Gels were imaged using a FluorChem R ProteinSimple imager.

BLI binding kinetics.

To measure the binding and dissociation kinetics of ClpXP, a BLI-based approach was used as described (Amor et al., 2016). All BLI assays were carried out in PD buffer at 30°C with 0.05% TWEEN-20 (Amresco). Single-chain ClpX$^{\Delta N}$ carrying a biotin-acceptor peptide was loaded onto streptavidin BLI surfaces to 0.5 nm loading signal. After washing with 2 mM ATP, BLI biosensors were transferred to 1 µM ClpP and 2 mM ATP to measure association kinetics. Surfaces were then transferred to 2 mM ATP lacking protein to measure dissociation kinetics. Data were initially fit to a single exponential equation to estimate half-lives. Data were then truncated to ~10 half-lives and re-fit to a single exponential or double-exponential equation.

Gel degradation assays of a multidomain substrate

A multidomain substrate consisting of a HaloLink enzyme, followed by the native I27 domain of titin, three concurring V13P I27 titin domains, and a C-terminal ssrA tag was used for gel degradation assays with ClpXP (Cordova et al. 2014). Substrate was purified as described for other protein reagents without ion exchange chromatography in 1 mM DTT (Amor et al. 2016). After purification substrate was desalted into 50 mM Tris pH 8.8, 150 mM NaCl, and 500x molar excess iodoacetic acid for 2 hr at 37 °C. Reactions were quenched in 5 mM DTT and exchanged into gel filtration buffer after size exclusion over a S200 column (GE) (Amor et al. 2016). Unfolding of V13P I27 domains was then assessed by gel filtration elution shift and W-fluorescence (Kenniston et al. 2003).

Degradation of this substrate was carried out in 1 μM ClpX, 2 μM ClpP, 10 mM ATP, 32 mM phosphocreatine, 0.064 mg/mL creatine kinase, and 10 μM substrate. Prior to addition of ATP, Halo-Tag-TMR was added for 15 min to label the multidomain substrate a the N-terminus covalently (Iosefson et al. 2015). 5 μL of reaction were taken at indicated time points and quenched in 2x Sample Buffer (Bio-Rad), boiled, and run over a 2-20% gradient gel (GenScript) in MOPS buffer (GenScript). Gels were rinsed 3x in ddH$_2$O, then imaged on a Typhoon FLA 9500 imager using the preset TARMA setting (GE).

References

Amor, A.J. et al., 2016. Highly Dynamic Interactions Maintain Kinetic Stability of the ClpXP Protease during the ATP-Fueled Mechanical Cycle. *ACS Chemical Biology*, 11,1552–1560.

Baker, T.A. & Sauer, R.T., 2012. ClpXP, an ATP-powered unfolding and protein-degradation machine. *Biochimica et Biophysica Acta - Molecular Cell Research*, 1823, 15–28.

Baytshtok, V., Baker, T.A. & Sauer, R.T., 2015. Assaying the kinetics of protein denaturation catalyzed by AAA+ unfolding machines and proteases. *Proceedings of the National Academy of Sciences*, 112, 5377–5382.

Conlon, B.P. et al., 2013. Activated ClpP kills persisters and eradicates a chronic biofilm infection. *Nature*, 503, 365–370.

Cordova, J.C. et al., 2014. Combining single-molecule manipulation and single-molecule detection. *Current Opinion in Structural Biology*, 28, 142–148.

Crooks, G. et al., 2004. WebLogo: a sequence logo generator. *Genome Res*, 14,1188–1190.

Farrell, C.M., Grossman, A.D. & Sauer, R.T., 2005. Cytoplasmic degradation of ssrA-tagged proteins. *Molecular Microbiology*, 57 1750–1761.

Glynn, S.E. et al., 2009. Structures of Asymmetric ClpX Hexamers Reveal Nucleotide-Dependent Motions in a AAA+ Protein-Unfolding Machine. *Cell*, 139, 744–756.

Hanson, P.I. & Whiteheart, S.W., 2005. AAA+ proteins: have engine, will work. *Nature Reviews. Molecular Cell Biology*, 6, 519–529.

Hersch, G.L. et al., 2005. Asymmetric interactions of ATP with the AAA+ ClpX6 unfoldase: Allosteric control of a protein machine. *Cell*, 121, 1017–1027.

Iosefson, O. et al., 2015. Dissection of axial-pore loop function during unfolding and translocation by a AAA+ proteolytic machine. *Cell Reports*, 12, 1032–1041.

Joshi, S. a et al., 2004. Communication between ClpX and ClpP during substrate processing and degradation. *Nature Structural & Molecular Biology*, 11, 404–411.

Keiler, K.C., Waller, P.R. & Sauer, R.T., 1996. Role of a peptide tagging system in degradation of proteins synthesized from damaged messenger RNA. *Science*, 271 990–993.

Kenniston, J.A. et al., 2003. Linkage between ATP Consumption and Mechanical Unfolding during the Protein Processing Reactions of an AAA+ Degradation Machine. *Cell*, 114, 511–520.

Kenniston, J.A., Baker, T.A. & Sauer, R.T., 2005. Partitioning between unfolding and release of

native domains during ClpXP degradation determines substrate selectivity and partial processing. *Proceedings of the National Academy of Sciences*, 102, 1390–1395.

Kim, D.Y. & Kim, K.K., 2003. Crystal Structure of ClpX Molecular Chaperone from Helicobacter pylori. *Journal of Biological Chemistry*, 278, 50664–50670.

Kim, Y.I. et al., 2000. Dynamics of substrate denaturation and translocation by the ClpXP degradation machine. *Molecular Cell*, 5, 639–648.

Kim, Y.I. et al., 2001. Molecular determinants of complex formation between Clp/Hsp100 ATPases and the ClpP peptidase. *Nature Structural Biology*, 8, 230–233.

Lee, B. et al., 2010a. Structures of ClpP in complex with acyldepsipeptide antibiotics reveal its activation mechanism. *Nature Structural & Molecular Biology*, 17, 471–478.

Lee, M.E., Baker, T.A. & Sauer, R.T., 2010b. Control of substrate gating and translocation into ClpP by channel residues and ClpX binding. *Journal of Molecular Biology*, 399, 707–718.

Martin, A., Baker, T.A. & Sauer, R.T., 2008. Diverse Pore Loops of the AAA+ ClpX Machine Mediate Unassisted and Adaptor-Dependent Recognition of ssrA-Tagged Substrates. *Molecular Cell*, 29, 441–450.

Martin, A., Baker, T. a. & Sauer, R.T., 2007. Distinct Static and Dynamic Interactions Control ATPase-Peptidase Communication in a AAA+ Protease. *Molecular Cell*, 27, 41–52.

Martin, A., Baker, T. a & Sauer, R.T., 2005. Rebuilt AAA + motors reveal operating principles for ATP-fuelled machines. *Nature*, 437, 1115–1120.

Nørby, J.G., 1988. Coupled assay of Na+,K+-ATPase activity. *Methods in Enzymology*, 156, 116–119.

Ortega, J. et al., 2002. Alternating translocation of protein substrates from both ends of ClpXP protease. *EMBO Journal*, 21, .4938–4949.

Schmitz, K.R. et al., 2014. Crystal structure of Mycobacterium tuberculosis ClpP1P2 suggests a model for peptidase activation by AAA+ partner binding and substrate delivery. *Proceedings of the National Academy of Sciences*, 111, E4587–E4595.

Singh, S.K. et al., 2001. Functional Domains of the ClpA and ClpX Molecular Chaperones Identified by Limited Proteolysis and Deletion Analysis. *Journal of Biological Chemistry*, 276, 29420–29429.

Stinson, B.M. et al., 2013. Nucleotide binding and conformational switching in the hexameric ring of a AAA+ machine. *Cell*, 153, 628–639.